Review

Recent Advances in Charmed Baryon Measurements at Belle and Belle II

Yuewen Zhong , Sen Jia * , Chengping Shen *

Posted Date: 6 February 2026

doi: 10.20944/preprints202602.0472.v1

Keywords: charmed baryons; Belle; Belle II; branching fractions; decay asymmetry; CP violation

Review

Recent Advances in Charmed Baryon Measurements at Belle and Belle II

Yuewen Zhong [1], Sen Jia [2,*], and Chengping Shen [1,3,*]

[1] Key Laboratory of Nuclear Physics and Ion-beam Application (MOE) and Institute of Modern Physics, Fudan University, Shanghai 200443, China
[2] School of Physics, Southeast University, Nanjing 211189, China
[3] School of Physics, Zhengzhou University, Zhengzhou 450001, China
* Correspondence: jiasen@seu.edu.cn (S.J.); shencp@fudan.edu.cn (C.S.)

Abstract

We review recent experimental progress in charmed baryon physics achieved by the Belle and Belle II experiments, with an emphasis on measurements reported since 2022. Using large e^+e^- data samples collected at or near the $\Upsilon(4S)$ resonance, Belle and Belle II have delivered a series of precision results on hadronic weak decays of anti-triplet charmed baryons, providing critical inputs for testing flavor-symmetry approaches and dynamical models. We summarize new and improved branching fraction determinations for Ξ_c^0, Ξ_c^+, and Λ_c^+ decays, including channels with neutral hadrons in the final state and the first measurements of several singly Cabibbo-suppressed modes. We also highlight the first determination of the decay asymmetry parameter in $\Xi_c^0 \to \Xi^0\pi^0$. In addition, we review the first Belle II measurements of CP asymmetries in three-body singly Cabibbo-suppressed decays of Ξ_c^+ and Λ_c^+, and discuss their implications for U-spin sum rules and searches for physics beyond the Standard Model. Finally, we look forward to exploiting the Belle II data set to perform more stringent tests of decay dynamics.

Keywords: charmed baryons; Belle; Belle II; branching fractions; decay asymmetry; CP violation

1. Introduction

The hadronic weak decays of baryons provide a powerful window into the dynamics of nonleptonic weak interactions in a strongly coupled, three-quark environment, and are closely connected to the fundamental problem of the cosmic matter–antimatter asymmetry [1,2]. Charmed baryons are especially valuable in this respect: their decays simultaneously test flavor symmetry ideas and expose genuinely nonperturbative quantum chromodynamics (QCD) effects that are difficult to control from first principles. Although a variety of phenomenological descriptions have been developed, including the widely used topological-diagram formalism [3], the complexity of heavy-flavored baryon decay dynamics continues to challenge any single quantitative framework [4]. As a result, precise experimental inputs are indispensable for discriminating among theoretical mechanisms and for pinning down the relative importance of factorizable and nonfactorizable contributions.

Experimentally, charmed baryon measurements are more challenging than their mesonic counterparts due to lower production rates; however, the situation has changed markedly with the advent of large data sets and improved detector performances. Over the past two decades, high-luminosity experiments have substantially enriched charmed baryon spectroscopy and motivated a new wave of precision studies of their decay properties [5]. In particular, absolute branching fraction measurements for key reference modes, including $\Lambda_c^+ \to pK^-\pi^+$, $\Xi_c^+ \to \Xi^-\pi^+\pi^+$, and $\Xi_c^0 \to \Xi^-\pi^+$, were performed at Belle [6–8]. Utilizing these absolute branching fractions as normalization channels, the absolute branching fractions for more Λ_c^+, Ξ_c^+, and Ξ_c^0 decay modes have been measured by Belle and Belle II in recent years [9–13]. Besides the branching fractions of charmed baryons in inclusive e^+e^-

 doi:10.20944/preprints202602.0472.v1

processes, Belle II reported a charmed baryon pair involving a sextet and an antitriplet from B decays for the first time [14].

For the weak decay of a spin-1/2 charmed baryon into a spin-0 meson and a spin-1/2 baryon, the decay asymmetry parameter α arises from the interference between parity-violating and parity-conserving amplitudes, reflecting both relative magnitudes and strong-phase differences [15]. Consequently, measurements of α probe the helicity structure and final-state-interaction effects that are not accessible through branching fractions alone. This makes precise determinations of α central to modern charmed baryon studies, as they complement rate measurements and sharpen tests of model-building assumptions [4]. Recently, Belle II measured the asymmetry parameter for $\Xi_c^0 \to \Xi^0\pi^0$ for the first time [9].

Searches for CP violation (CPV) in charmed baryon decays are particularly compelling. CP violation is one of the necessary ingredients for generating the observed matter–antimatter asymmetry in the Universe [2,16,17]. Within the Standard Model (SM), CPV originates from a single complex phase in the CKM matrix, yet its predicted magnitude is insufficient to account for the cosmological asymmetry. Although CPV has been firmly established in open-flavor mesons, it remains unconfirmed for charmed baryons. Recent progress in the baryon sector, including the observation of CPV in beauty-baryon decays [18], further motivates extending sensitive searches to charm. In practice, CPV can appear both as a decay-rate asymmetry and through polarization-related observables; for two-body decays, the latter is naturally accessed via α-based asymmetries [15]. Moreover, because SM expectations for CPV in charm are typically very small, an observed effect at the level significantly above 10^{-3} would provide a strong hint of physics beyond the SM [19–23]. Phenomenological investigations of CPV in charmed baryons exist but remain limited, underscoring the importance of new high-precision measurements [24–27]. Recently, Belle II searched for CP violation in $\Xi_c^+ \to \Sigma^+K^+K^-$, $\Xi_c^+ \to \Sigma^+\pi^+\pi^-$, $\Lambda_c^+ \to pK^+K^-$, and $\Lambda_c^+ \to p\pi^+\pi^-$ for the first time [28].

Motivated by these considerations, and in light of the recent experimental progress, this review summarizes the most up-to-date measurements of branching fractions, decay asymmetry parameters, and CPV searches in charmed baryon decays, with an emphasis on results reported since 2022 [9–14,28], and compares them with representative theoretical expectations. The remainder of this paper is organized as follows. Section 2 briefly introduces the Belle and Belle II experiments and datasets. Sections 3 and 4 review recent branching fraction measurements in inclusive e^+e^- processes and in B-meson decays, respectively. Sections 5 and 6 summarize recent results on decay asymmetry parameters and CP asymmetries. Finally, Section 7 presents a summary and outlook.

2. Belle and Belle II Experiments

The Belle experiment is an international collaborative particle-physics experiment, conducted at the High Energy Accelerator Research Organization (KEK) in Japan, using the KEKB asymmetric-energy electron–positron collider. As one of the world's leading B-factory experiments, Belle was designed and optimized to precisely measure CP-violation phenomena in the B-meson system. In the experiment, electrons and positrons are accelerated by KEKB to energies close to the speed of light and brought into collision at the interaction point, where the Belle detector records the particles produced in the annihilation process [29,30]. The Belle experiment began data taking in 1999 and, by 2010, had collected an integrated luminosity of approximately 1 ab^{-1} [31]. Its primary physics goals include studies of B-meson mixing, decays, and CP-violation phenomena, while also covering charm physics, τ physics, and other rare processes. In 2001, Belle (together with the BaBar experiment) observed CP violation in B-meson decays [32], a result consistent with the theoretical predictions of Kobayashi and Maskawa, and this achievement was explicitly cited in the award of the 2008 Nobel Prize in Physics [31].

The Belle II experiment is an upgraded successor to Belle and represents a new-generation super B factory [33]. Its main scientific objectives include high-precision measurements of flavor-interaction parameters, in-depth studies of charm physics, and searches for physics beyond the SM [34]. From

 doi:10.20944/preprints202602.0472.v1

2019 to 2022, during its first phase of operation (Run 1), Belle II successfully collected data with an integrated luminosity of 428 fb^{-1} [35]. From 2024, Belle II started the second phase of operation (Run 2). On December 27, 2024, it achieved a record instantaneous luminosity of 5.1×10^{34} cm^{-2}s^{-1}, marking the entry of the experiment into a new era of high-precision physics studies. The combined data samples from the Belle and Belle II experiments correspond to an integrated luminosity of 1.6 ab^{-1}. The abundant data samples for studies of B and charm hadrons as well as for rare-process searches. In addition, the experiment also involves investigations related to hadron physics and dark matter.

The data collected by the Belle and Belle II experiments are primarily taken at the center-of-mass (C.M.) energy $\sqrt{s} = 10.58$ GeV, corresponding to the production of the $\Upsilon(4S)$ resonance, which predominantly decays into $B\bar{B}$ pairs. In addition to $\Upsilon(4S)$ production, the electron–positron annihilation process also yields abundant charm hadrons at $\sqrt{s} = 10.58$ GeV. Table 1 summarizes the reaction cross sections for various physics processes produced in e^+e^- collisions at $\sqrt{s} = 10.58$ GeV. As a result, the Belle and Belle II experiments serve not only as B factories but also as important platforms for charm-physics research.

Table 1. Reaction cross sections of various physics processes produced in e^+e^- annihilation at $\sqrt{s} = 10.58$ GeV [34].

Process	Cross section (nb)
$e^+e^- \to \Upsilon(4S)$	1.05 ± 0.10
$e^+e^- \to c\bar{c}$	1.329
$e^+e^- \to q\bar{q}$ $(q = u, d, s)$	2.339
$e^+e^- \to \tau^+\tau^-(\gamma)$	0.919
$e^+e^- \to \mu^+\mu^-(\gamma)$	1.148
$e^+e^- \to e^+e^-(\gamma)$	300 ± 3

3. Branching Fractions of Charmed Baryons in Inclusive e^+e^- Processes

In the last decade, experimental investigations of charmed baryons have achieved substantial progress [36]. In particular, absolute branching fractions have been established for several benchmark decay modes, including $\Lambda_c^+ \to pK^-\pi^+$ [6], $\Xi_c^+ \to \Xi^-\pi^+\pi^+$ [8], and $\Xi_c^0 \to \Xi^-\pi^+$ [7]. Throughout these measurements, charge-conjugate processes are implicitly taken into account. The availability of these absolute measurements has laid the groundwork for extracting branching fractions of anti-triplet charmed baryons in a wide range of decay channels.

3.1. Studies of Ξ_c^0 Decays

In recent years, an increasing number of theoretical predictions have been made within various dynamical models [37–43] and the framework of SU(3) flavor symmetry [44–52]. These theoretical approaches have been widely applied to predict the branching fractions of Cabibbo-favored (CF) and Cabibbo-suppressed (CS) decays, including decay modes of the $\Xi_c^0 \to \Xi^0 h^0$ (CF) and $\Xi_c^0 \to \Lambda h^0$ (CS), where $h^0 = \pi^0$, η, and η'. Figure 1 illustrates the Feynman diagrams for the internal W-emission and W-exchange topologies contributing to the CF decays $\Xi_c^0 \to \Xi^0 h^0$, in which only nonfactorizable amplitudes contribute [5]. For the decay $\Xi_c^0 \to \Lambda h^0$, the relevant topological contributions can be expressed in a compact form, as shown in Figure 2.

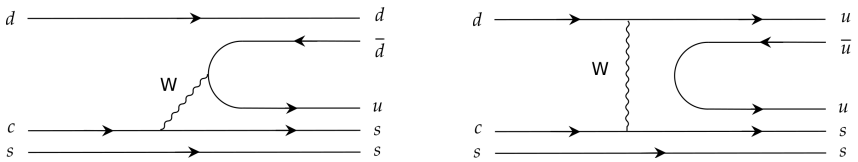

Figure 1. The Feynman diagrams for (left) internal W-emission and (right) W-exchange in $\Xi_c^0 \to \Xi^0 h^0$ decays [5].

 doi:10.20944/preprints202602.0472.v1

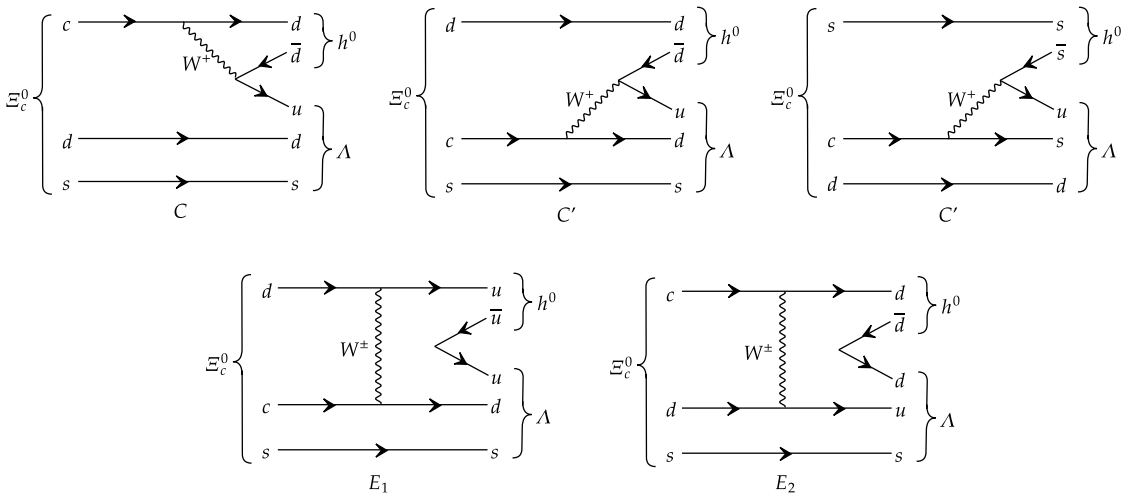

Figure 2. Topological diagrams contributing to $\Xi_c^0 \to \Lambda h^0$ decays: internal W-emission C, inner W-emission C', and W-exchange diagrams E_1 and E_2 [5].

In 2024, Belle II reported measurements of the branching fractions for the CF decay modes $\Xi_c^0 \to \Xi^0 h^0$ with $h^0 = \pi^0$, η, and η', providing new experimental inputs from charmed baryons including neutral final states [9]. The invariant mass distributions are shown in Figure 3. The signal yields for $\Xi_c^0 \to \Xi^0\pi^0$, $\Xi_c^0 \to \Xi^0\eta$, and $\Xi_c^0 \to \Xi^0\eta'$ are 1315±66 (869±46), 81±15 (60±11), 23±6 (8±4) at Belle (Belle II), respectively. The statistical significances for $\Xi_c^0 \to \Xi^0\pi^0$, $\Xi_c^0 \to \Xi^0\eta$, and $\Xi_c^0 \to \Xi^0\eta'$ are greater than 10σ (10σ), 6.2σ (6.7σ), and 5.9σ (2.4σ) at Belle (Belle II), respectively. The ratios of branching fractions to the normalization mode $\Xi_c^0 \to \Xi^-\pi^+$ were calculated to be

$$\frac{\mathcal{B}(\Xi_c^0 \to \Xi^-\pi^0)}{\mathcal{B}(\Xi_c^0 \to \Xi^-\pi^+)} = 0.48 \pm 0.02 \pm 0.03, \tag{1}$$

$$\frac{\mathcal{B}(\Xi_c^0 \to \Xi^-\eta)}{\mathcal{B}(\Xi_c^0 \to \Xi^-\pi^+)} = 0.11 \pm 0.01 \pm 0.01, \tag{2}$$

$$\frac{\mathcal{B}(\Xi_c^0 \to \Xi^-\eta')}{\mathcal{B}(\Xi_c^0 \to \Xi^-\pi^+)} = 0.08 \pm 0.02 \pm 0.01. \tag{3}$$

where the first and second uncertainties are statistical and systematic throughout this review. Using the branching fraction of the normalization mode, $\mathcal{B}(\Xi_c^0 \to \Xi^-\pi^+) = (1.43 \pm 0.27)\%$ [36], Belle II obtained the absolute branching fractions, which are listed in Table 2. The experimental results were compared with theoretical expectations, as shown in Figure 4, allowing for stringent tests of various theoretical models.

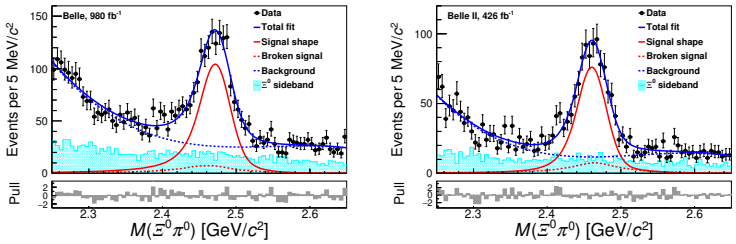

Figure 3. *Cont.*

 doi:10.20944/preprints202602.0472.v1

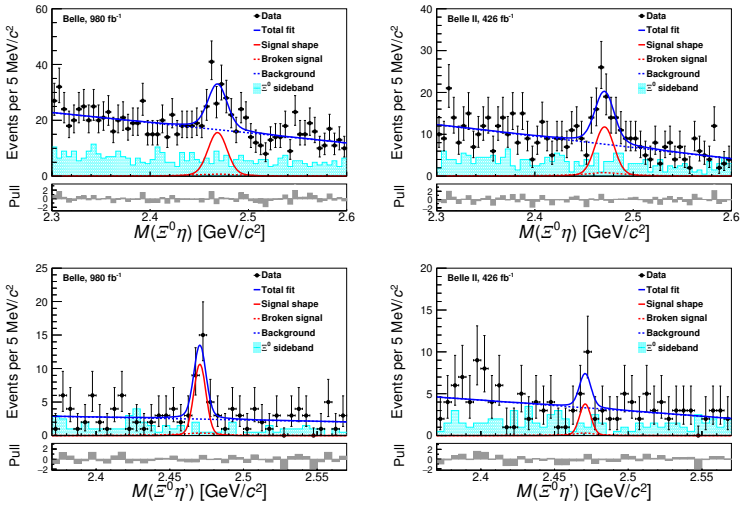

Figure 3. invariant mass distributions of Ξ_c^0 candidates in data samples for $\Xi_c^0 \to \Xi^0\pi^0$, $\Xi_c^0 \to \Xi^0\eta$, and $\Xi_c^0 \to \Xi^0\eta'$ modes from the (left) Belle and (right) Belle II experiments [9]. The markers with error bars represent the data. The solid blue curves, solid red curves, dashed red curves, and dashed blue curves show the total fit, signal shape, broken-signal shape, and smooth backgrounds, respectively. The cyan histograms show the data from the Ξ^0 mass sidebands.

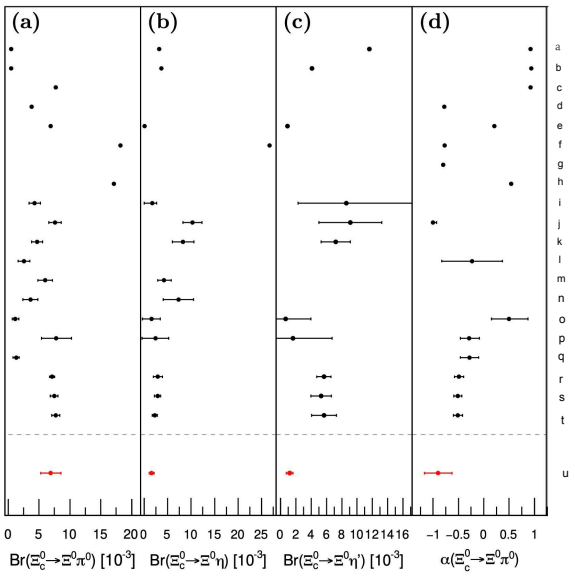

Figure 4. Comparisons of the measured $\mathcal{B}(\Xi_c^0 \to \Xi^0\pi^0)$, $\mathcal{B}(\Xi_c^0 \to \Xi^0\eta)$, $\mathcal{B}(\Xi_c^0 \to \Xi^0\eta')$, and $\alpha(\Xi_c^0 \to \Xi^0\pi^0)$ with theoretical predictions. The dots and error bars represent the central values and uncertainties, respectively. Dots without error bars indicate that no theoretical uncertainty is available. The theoretical results correspond to: (a) Körner and Krämer [37], (quark model); (b) Ivanov *et al.* [38], (quark model); (c) Xu and Kamal [39], (pole model); (d) Cheng and Tseng [40], (pole model); (e) Żenczykowski [41], (pole model); (f) Zou *et al.* [42], (pole model); (g) Sharma and Verma [43], (current algebra); (h) Cheng and Tseng [40], (current algebra); (i) Geng *et al.* [44], $(SU(3)_F$ symmetry(IRA)); (j) Geng *et al.* [45], $(SU(3)_F$ symmetry(IRA)); (k) Zhao *et al.* [50], $(SU(3)_F$ symmetry(TDA)); (l) Huang *et al.* [46], $(SU(3)_F$ symmetry(IRA)); (m) Hsiao *et al.* [51], $(SU(3)_F$ symmetry(TDA)); (n) Hsiao *et al.* [51], $(SU(3)_F$-breaking (TDA)); (o) Zhong *et al.* [47], $(SU(3)_F$ symmetry(IRA)); (p) Zhong *et al.* [47], $(SU(3)_F$-breaking (IRA)); (q) Xing *et al.* [49], $(SU(3)_F$ symmetry(IRA)); (r) Geng *et al.* [53], $(SU(3)_F$ symmetry(KPW)); (s) Zhong *et al.* (I) [52], $(SU(3)_F$ (TDA)); (t) Zhong *et al.* (II) [52], $(SU(3)_F$ (IRA)). and (u) the Belle and Belle II combined measurements. Throughout this review, the TDA represents topological diagram approach, and the IRA represents irreducible representation amplitude. The KPW impose the Körner–Pati–Woo theorem, which restricts certain decay amplitudes due to the antisymmetry of diquark configurations.

 doi:10.20944/preprints202602.0472.v1

Table 2. Recent Belle II measurements of the branching fractions $\mathcal{B}$ of charmed baryons. The first and second uncertainties are statistical and systematic, respectively, while the third uncertainty arises from that of the reference mode.

Decay	$\mathcal{B}$
$\Xi_c^0 \to \Lambda\pi^0$	$< 5.2 \times 10^{-4}$ (90% C.L.)
$\Xi_c^0 \to \Lambda\eta$	$(5.95 \pm 1.30 \pm 0.32 \pm 1.13) \times 10^{-4}$
$\Xi_c^0 \to \Lambda\eta'$	$(3.55 \pm 1.17 \pm 0.17 \pm 0.68) \times 10^{-4}$
$\Xi_c^0 \to \Xi^0\pi^0$	$(6.9 \pm 0.3 \pm 0.5 \pm 1.5) \times 10^{-3}$
$\Xi_c^0 \to \Xi^0\eta$	$(1.6 \pm 0.2 \pm 0.2 \pm 0.4) \times 10^{-3}$
$\Xi_c^0 \to \Xi^0\eta'$	$(1.2 \pm 0.3 \pm 0.1 \pm 0.3) \times 10^{-3}$
$\Xi_c^+ \to pK_S^0$	$(7.16 \pm 0.46 \pm 0.20 \pm 3.21) \times 10^{-4}$
$\Xi_c^+ \to \Lambda\pi^+$	$(4.52 \pm 0.41 \pm 0.26 \pm 2.03) \times 10^{-4}$
$\Xi_c^+ \to \Sigma^0\pi^+$	$(1.20 \pm 0.08 \pm 0.07 \pm 0.54) \times 10^{-3}$
$\Xi_c^+ \to \Sigma^+K_S^0$	$(0.186 \pm 0.020 \pm 0.009 \pm 0.083)\%$
$\Xi_c^+ \to \Xi^0\pi^+$	$(0.677 \pm 0.024 \pm 0.030 \pm 0.303)\%$
$\Xi_c^+ \to \Xi^0K^+$	$(0.046 \pm 0.007 \pm 0.002 \pm 0.021)\%$
$\Lambda_c^+ \to pK_S^0\pi^0$	$(2.12 \pm 0.01 \pm 0.05 \pm 0.10)\%$

In 2025, Belle II reported the branching fraction for the singly Cabibbo-suppressed (SCS) decay $\Xi_c^0 \to \Lambda h^0$ [10]. The invariant mass distributions are shown in Figure 5. Fits to data combining Belle and Belle II return signal yields of 262 ± 57, 101 ± 33, and 190 ± 120 events for the $\Xi_c^0 \to \Lambda\eta$, $\Xi_c^0 \to \Lambda\eta'$, and $\Xi_c^0 \to \Lambda\pi^0$ decay modes, corresponding to statistical significances of 5.1σ, 3.2σ, and 1.4σ, respectively. The measured branching ratios for $\Xi_c^0 \to \Lambda\eta$ and $\Xi_c^0 \to \Lambda\eta'$ are

$$\frac{\mathcal{B}(\Xi_c^0 \to \Lambda\eta)}{\mathcal{B}(\Xi_c^0 \to \Xi^-\pi^+)} = (4.16 \pm 0.91 \pm 0.23)\%, \tag{4}$$

and

$$\frac{\mathcal{B}(\Xi_c^0 \to \Lambda\eta')}{\mathcal{B}(\Xi_c^0 \to \Xi^-\pi^+)} = (2.48 \pm 0.82 \pm 0.12)\%. \tag{5}$$

Belle II find no evidence for the decay $\Xi_c^0 \to \Lambda\pi^0$ and set an upper limit at the 90% confidence level (C.L.) of

$$\frac{\mathcal{B}(\Xi_c^0 \to \Lambda\pi^0)}{\mathcal{B}(\Xi_c^0 \to \Xi^-\pi^+)} < 3.5\%. \tag{6}$$

Branching ratios obtained from independent fits to Belle and Belle II data are consistent with those obtained from simultaneous fits. Using the branching fraction of the normalization mode, $\mathcal{B}(\Xi_c^0 \to \Xi^-\pi^+) = (1.43 \pm 0.27)\%$ [36], Belle II obtained the absolute branching fractions, which are listed in Table 2. The corresponding experimental results were compared with theoretical expectations, as shown in Figure 6.

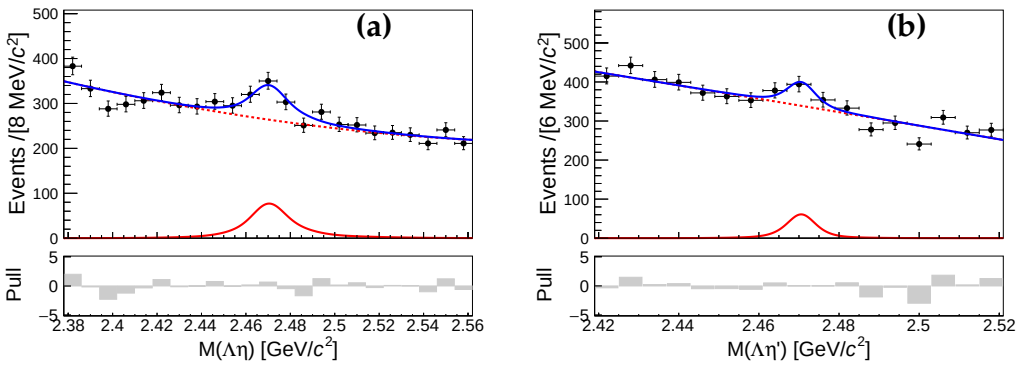

Figure 5. *Cont.*

 doi:10.20944/preprints202602.0472.v1

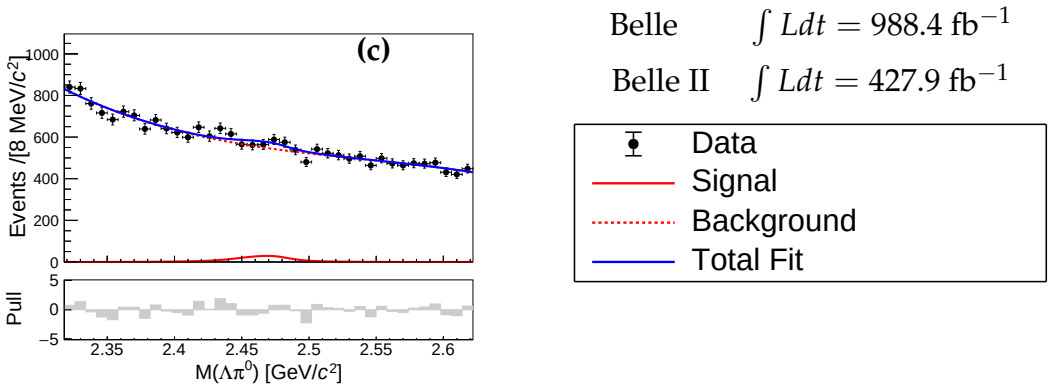

Figure 5. The invariant mass spectra of (a) $\Lambda\eta$, (b) $\Lambda\eta'$, and (c) $\Lambda\pi^0$ candidates overlaid with the fit results obtained using the Belle and Belle II data samples [10]. Dots with error bars represent the number of events in data; solid red curves indicate the signal probability density functions; dashed red lines denote the fitted combinatorial backgrounds; solid blue curves illustrate the fit results. The gray bars show the pull distributions of the fit results.

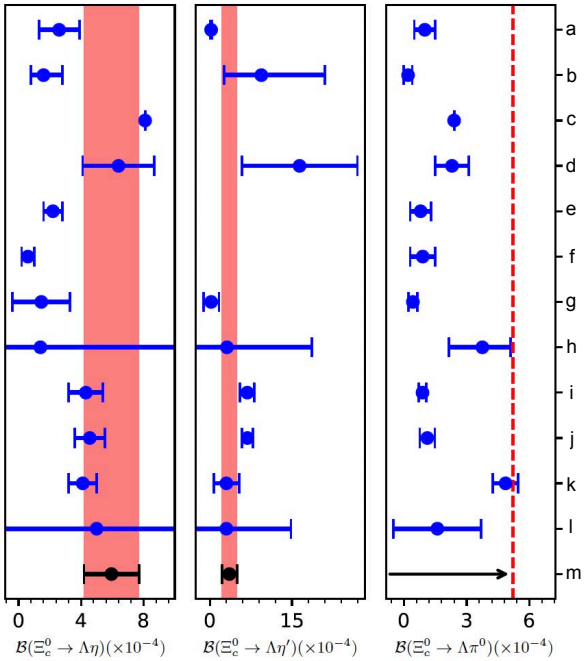

Figure 6. Comparison of the branching fractions $\mathcal{B}(\Xi_c^0 \to \Lambda\eta)$, $\mathcal{B}(\Xi_c^0 \to \Lambda\eta')$, and the measured 90% C.L. upper limit on $\mathcal{B}(\Xi_c^0 \to \Lambda\pi^0)$ with respect to theoretical predictions [42,44,45,47,49–53]. Dots with error bars represent central values and their uncertainties; those without error bars indicate that no theoretical uncertainty is provided. Missing dots signify the absence of theoretical predictions for the corresponding decay mode. Some predictions exhibit large errors that are not fully shown within the present scale. The black dots with error bars denote the measured absolute branching fractions of the decays $\Xi_c^0 \to \Lambda\eta$ and $\Xi_c^0 \to \Lambda\eta'$. The red vertical bands denote the $\pm 1\sigma$ intervals dominated by the systematic uncertainty of $\mathcal{B}(\Xi_c^0 \to \Xi^-\pi^+)$. The red dashed line and black arrow indicate the measured 90% C.L. upper limits on $\mathcal{B}(\Xi_c^0 \to \Lambda\pi^0)$. The meanings of the vertical coordinates (a)-(m) in the figure: (a) Zhao *et al.* [50], ($SU(3)_F$ symmetry, TDA); (b) Geng *et al.* [44], ($SU(3)_F$ symmetry, IRA); (c) Zou *et al.* [42], (pole model); (d) Geng *et al.* [45], ($SU(3)_F$ symmetry, IRA); (e) Hsiao *et al.* (I) [51], ($SU(3)_F$ symmetry, TDA); (f) Hsiao *et al.* (II) [51], ($SU(3)_F$-breaking, TDA); (g) Zhong *et al.* (I) [47], ($SU(3)_F$ symmetry, IRA); (h) Zhong *et al.* (II) [47], ($SU(3)_F$-breaking, IRA); (i) Geng *et al.* [53], ($SU(3)_F$ symmetry, KPW); (j) Zhong *et al.* [52], ($SU(3)_F$, TDA); (k) Xing *et al.* (I) [49], ($SU(3)_F$, IRA, real form factors); (l) Xing *et al.* (II) [49], ($SU(3)_F$, IRA, complex form factors); (m) Belle and Belle II combined measurements. For Ref. [49], (I) and (II) denote the predicted values obtained using real form factors only and those incorporating complex form factors, respectively.

 doi:10.20944/preprints202602.0472.v1

3.2. Studies of Ξ_c^+ Decays

The weak decays of the Ξ_c^+ baryon have been extensively studied within various dynamical models [42] and SU(3)-based frameworks [44–48,50–54]. The corresponding theoretical predictions differ substantially among these approaches, highlighting the crucial role of experimental measurements in constraining and refining theoretical descriptions of Ξ_c^+ decays. However, most decay channels remain experimentally unmeasured, particularly the SCS modes. Figure 7 illustrates the typical decay diagrams arising from internal W-emission and W-exchange contributions for the SCS decays $\Xi_c^+ \to pK_S^0$, $\Xi_c^+ \to \Lambda\pi^+$, and $\Xi_c^+ \to \Sigma^0\pi^+$. Notably, the decay $\Xi_c^+ \to pK_S^0$ proceeds through purely nonfactorizable diagrams, so its measurement provides a direct probe of their importance in Ξ_c^+ decays. Predictions from different theoretical models place the branching fractions of these channels in the range of 10^{-4} to 10^{-3} [42,44–48,50–54].

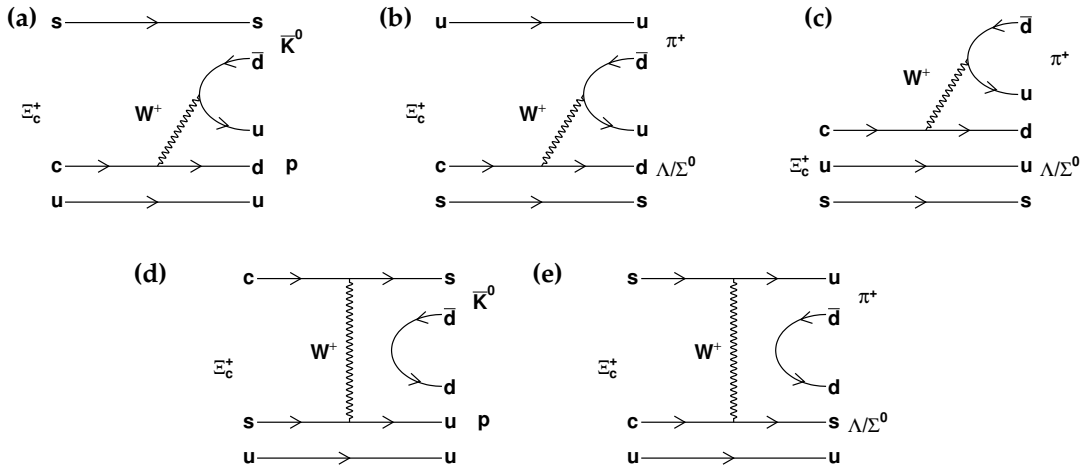

Figure 7. Typical decay diagrams from (a,b) internal W-emission, (c) external W-emission, and (d,e) W-exchange contributions for the SCS decays $\Xi_c^+ \to p\bar{K}^0$, $\Xi_c^+ \to \Lambda\pi^+$, and $\Xi_c^+ \to \Sigma^0\pi^+$.

In 2024, Belle II measured the branching fractions of these three SCS decay modes $\Xi_c^+ \to pK_S^0$, $\Xi_c^+ \to \Lambda\pi^+$, and $\Xi_c^+ \to \Sigma^0\pi^+$ [11]. The invariant mass distributions are shown in Figure 8. The signal yields for the decays $\Xi_c^+ \to pK_S^0$, $\Xi_c^+ \to \Lambda\pi^+$, and $\Xi_c^+ \to \Sigma^0\pi^+$ are 917 ± 103 (608 ± 45), 530 ± 88 (275 ± 30), and 537 ± 57 (359 ± 27) events at Belle (Belle II), respectively. Each signal has a significance greater than 10σ, using the combined data samples collected by the Belle and Belle II detectors. The ratios of branching fractions relative to the normalization mode $\Xi_c^+ \to \Xi^-\pi^+\pi^+$ are determined to be

$$\frac{\mathcal{B}(\Xi_c^+ \to pK_S^0)}{\mathcal{B}(\Xi_c^+ \to \Xi^-\pi^+\pi^+)} = (2.47 \pm 0.16 \pm 0.07)\%, \tag{7}$$

$$\frac{\mathcal{B}(\Xi_c^+ \to \Lambda\pi^+)}{\mathcal{B}(\Xi_c^+ \to \Xi^-\pi^+\pi^+)} = (1.56 \pm 0.14 \pm 0.09)\%, \tag{8}$$

and

$$\frac{\mathcal{B}(\Xi_c^+ \to \Sigma^0\pi^+)}{\mathcal{B}(\Xi_c^+ \to \Xi^-\pi^+\pi^+)} = (4.13 \pm 0.26 \pm 0.22)\%. \tag{9}$$

Using the branching fraction of the normalization mode, $\mathcal{B}(\Xi_c^+ \to \Xi^-\pi^+\pi^+) = (2.9 \pm 1.3)\%$ [36], Belle II obtained the absolute branching fractions. The results are summarized in Table 2 and compared with theoretical expectations in Figure 9.

 doi:10.20944/preprints202602.0472.v1

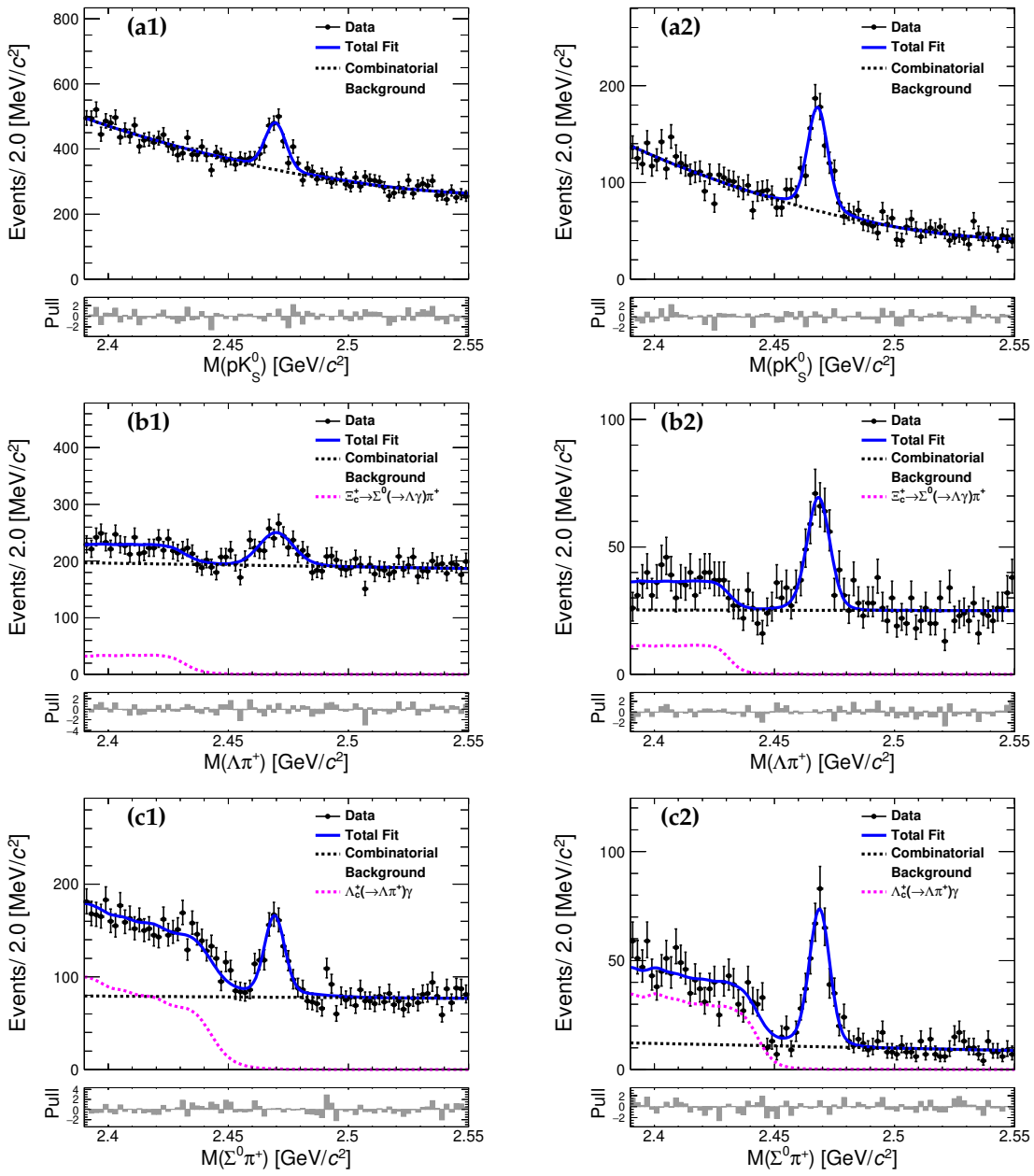

Figure 8. invariant mass spectra of (a) pK_S^0, (b) $\Lambda\pi^+$, and (c) $\Sigma^0\pi^+$ in the (1) Belle and (2) Belle II data [11]. The points with error bars represent the data, the solid blue curves show the best-fit results, and the black dashed curves represent the fitted combinatorial backgrounds. In the $M(\Lambda\pi^+)$ and $M(\Sigma^0\pi^+)$ distributions, the pink dashed curves indicate the fitted feed-down backgrounds from the $\Xi_c^+ \to \Sigma^0(\to \Lambda\gamma)\pi^+$ and $\Lambda_c^+ \to \Lambda\pi^+$ decays, respectively.

 doi:10.20944/preprints202602.0472.v1

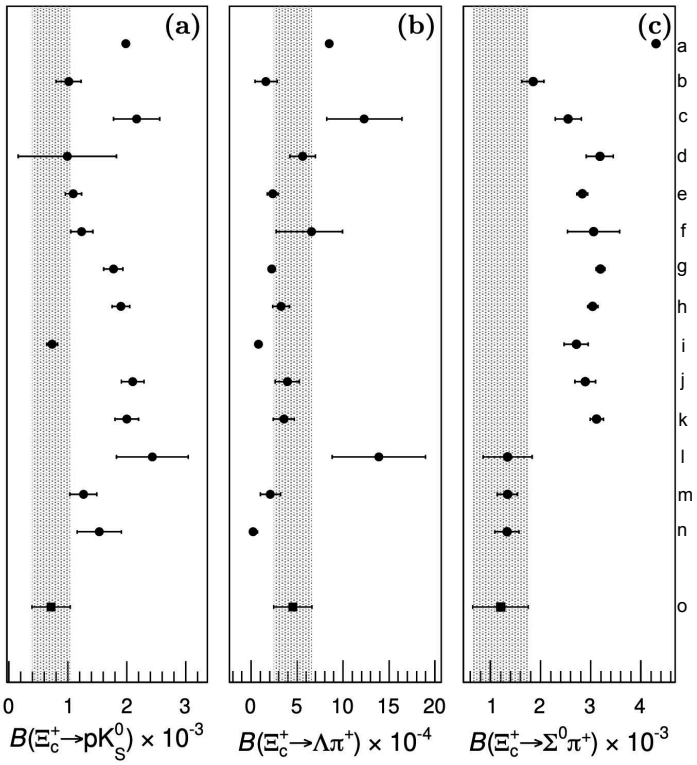

Figure 9. Comparisons of the measured (a) $\mathcal{B}(\Xi_c^+ \to pK_S^0)$, (b) $\mathcal{B}(\Xi_c^+ \to \Lambda\pi^+)$, and (c) $\mathcal{B}(\Xi_c^+ \to \Sigma^0\pi^+)$ with theoretical predictions. The dots and error bars represent the central values and uncertainties of the theoretical predictions, respectively. The dots without error bars indicate that no theoretical uncertainty is available. The squares and error bars denote the measured central values and uncertainties in this work. The meanings of the vertical coordinates (a)-(o) in the figure: (a) Zou *et al.* [42], (pole model); (b) Geng *et al.* [44], ($SU(3)_F$ symmetry (IRA)); (c) Geng *et al.* [45], ($SU(3)_F$ symmetry (IRA)); (d) Huang *et al.* [46], ($SU(3)_F$ symmetry (IRA)); (e) Zhong *et al.* (I) [47], ($SU(3)_F$ symmetry (IRA)); (f) Zhong *et al.* (II) [47], ($SU(3)_F$-breaking (IRA)); (g) Xing *et al.* [48], ($SU(3)_F$ symmetry (IRA)); (h) Geng *et al.* [53], ($SU(3)_F$ with KPW constraint); (i) Liu [54], ($SU(3)_F$ symmetry (IRA)); (j) Zhong *et al.* (I) [52], ($SU(3)_F$ (TDA)); (k) Zhong *et al.* (II) [52], ($SU(3)_F$ (IRA)); (l) Zhao *et al.* [50], ($SU(3)_F$ symmetry (TDA)); (m) Hsiao *et al.* (I) [51], ($SU(3)_F$ symmetry (TDA)); (n) Hsiao *et al.* (II) [51], ($SU(3)_F$-breaking (TDA)); (o) Belle and Belle II combined.

Beyond SCS decays, theoretical studies also predict sizable branching fractions for several CF modes of Ξ_c^+. In particular, the CF decay $\Xi_c^+ \to \Sigma^+ K_S^0$ is predicted to have a branching fraction of order 10^{-2} [42,45–48,50,51,54], yet had not been measured previously, motivating its first experimental study. For another CF decay, $\Xi_c^+ \to \Xi^0\pi^+$, earlier measurements suffered from substantial uncertainties [55], while the more recent results from Belle and Belle II provide a significantly improved determination of the branching fraction. Meanwhile, the SCS decay $\Xi_c^+ \to \Xi^0 K^+$ is predicted to have a branching fraction in the range 10^{-3}–10^{-2} [42,45–48,50,51,54]. Given its experimental similarity to $\Xi_c^+ \to \Xi^0\pi^+$, it was also searched for in the Belle and Belle II data samples.

In 2025, Belle II reported the first measurements of the branching fractions for $\Xi_c^+ \to \Sigma^+ K_S^0$ and $\Xi_c^+ \to \Xi^0 K^+$, together with an improved determination of the branching fraction for $\Xi_c^+ \to \Xi^0\pi^+$, using $\Xi_c^+ \to \Xi^-\pi^+\pi^+$ as the normalization mode [12]. The invariant mass distributions are shown in Figure 10. The signal yields for $\Xi_c^+ \to \Sigma^+ K_S^0$, $\Xi_c^+ \to \Xi^0\pi^+$, and $\Xi_c^+ \to \Xi^0 K^+$ are 286±40 (178±31), 2728±165 (1419±63), 134±30 (94±19) at Belle (Belle II), respectively. The statistical significances for $\Xi_c^+ \to \Sigma^+ K_S^0$, $\Xi_c^+ \to \Xi^0\pi^+$, and $\Xi_c^+ \to \Xi^0 K^+$ are 7.4σ (5.7σ), greater than 10σ (10σ), and 4.7σ (5.4σ) at Belle (Belle II), respectively. The branching fractions relative to $\mathcal{B}(\Xi_c^+ \to \Xi^-\pi^+\pi^+)$ are measured to be

$$\frac{\mathcal{B}(\Xi_c^+ \to \Sigma^+ K_S^0)}{\mathcal{B}(\Xi_c^+ \to \Xi^-\pi^+\pi^+)} = 0.064 \pm 0.007 \ \pm 0.003, \tag{10}$$

 doi:10.20944/preprints202602.0472.v1

$$\frac{\mathcal{B}(\Xi_c^+ \to \Xi^0\pi^+)}{\mathcal{B}(\Xi_c^+ \to \Xi^-\pi^+\pi^+)} = 0.233 \pm 0.008 \ \pm 0.010, \tag{11}$$

and

$$\frac{\mathcal{B}(\Xi_c^+ \to \Xi^0 K^+)}{\mathcal{B}(\Xi_c^+ \to \Xi^-\pi^+\pi^+)} = 0.016 \pm 0.002 \ \pm 0.001. \tag{12}$$

Using the branching fraction of the normalization mode, $\mathcal{B}(\Xi_c^+ \to \Xi^-\pi^+\pi^+) = (2.9 \pm 1.3)\%$ [36], Belle II obtained the absolute branching fractions. These results, summarized in Table 2 and compared with theoretical predictions in Figure 11, provide valuable tests of different theoretical models.

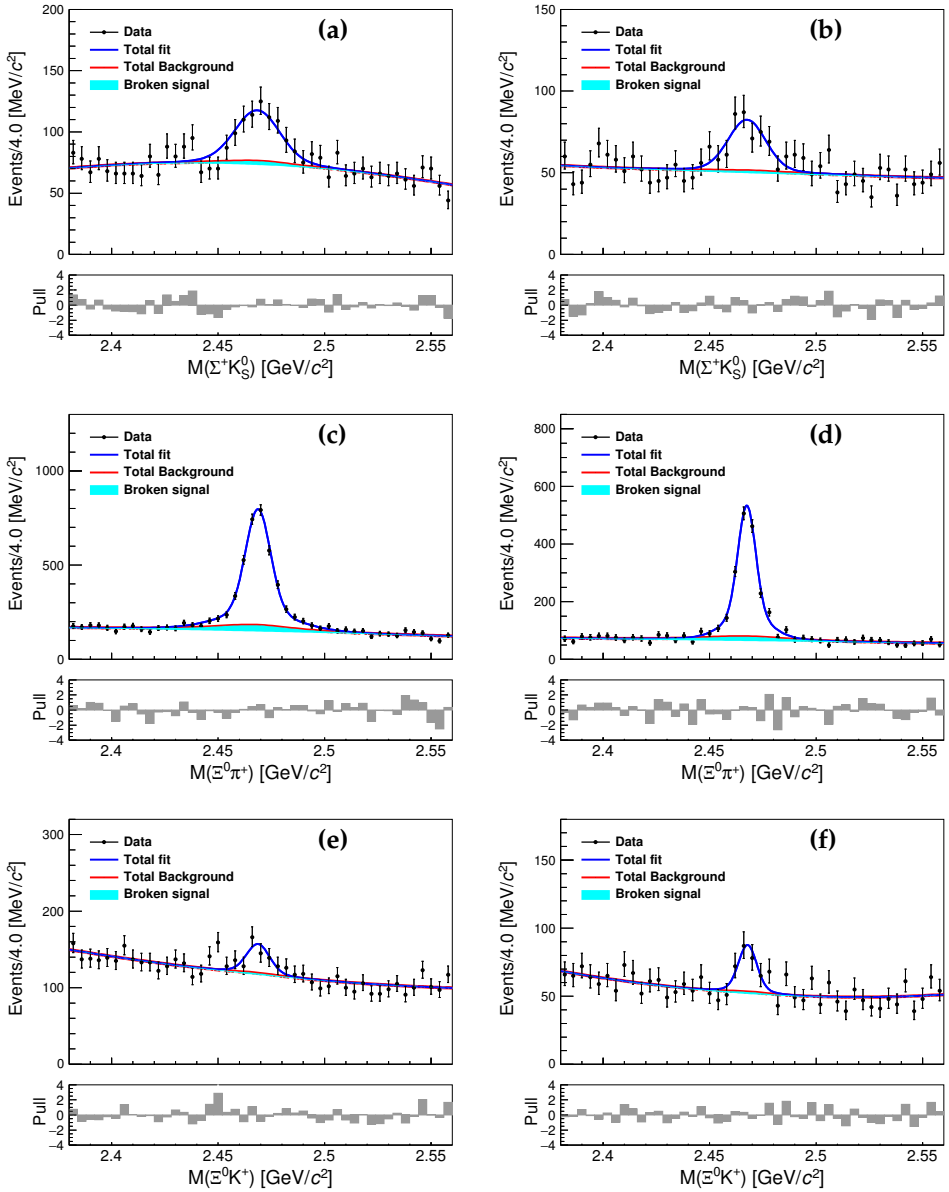

Figure 10. invariant mass distributions of Ξ_c^+ candidates from (a) $\Xi_c^+ \to \Sigma^+ K_S^0$, (b) $\Xi_c^+ \to \Xi^0\pi^+$, and (c) $\Xi_c^+ \to \Xi^0 K^+$ decays reconstructed in the (left) Belle and (right) Belle II data [12]. The black dots with error bars represent the distributions from data. The solid blue and red curves show the total fit and total background, respectively. The cyan areas indicate the broken-signal component.

 doi:10.20944/preprints202602.0472.v1

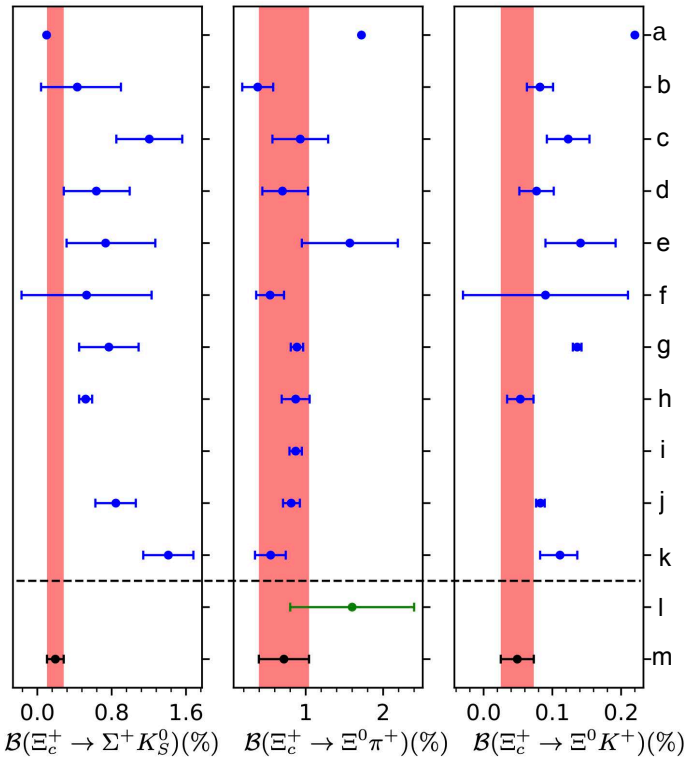

Figure 11. Comparison of the measured branching fractions $\mathcal{B}(\Xi_c^+ \to \Sigma^+ K_S^0)$, $\mathcal{B}(\Xi_c^+ \to \Xi^0 \pi^+)$, and $\mathcal{B}(\Xi_c^+ \to \Xi^0 K^+)$ with theoretical predictions. The blue dots with error bars represent theoretical predictions. The green dot with an error bar indicates the result from CLEO, and the black dots with error bars correspond to the results of this study. The meanings of the vertical coordinates (a)-(m) in the figure: (a) Zou *et al.* [42], (pole model); (b) Geng *et al.* [45], ($SU(3)_F$ symmetry (IRA)); (c) Zhao *et al.* [50], ($SU(3)_F$ symmetry (TDA)); (d) Hsiao *et al.* (I) [51], ($SU(3)_F$ symmetry (TDA)); (e) Hsiao *et al.* (II) [51], ($SU(3)_F$-breaking (TDA)); (f) Huang *et al.* [46], ($SU(3)_F$ symmetry (IRA)); (g) Xing *et al.* [48], ($SU(3)_F$ symmetry (IRA)); (h) Liu *et al.* (I) [54], ($SU(3)_F$ symmetry (IRA)); (i) Liu *et al.* (II) [54], ($SU(3)_F$-breaking (IRA)); (j) Zhong *et al.* (I) [47], ($SU(3)_F$ symmetry (IRA)); (k) Zhong *et al.* (II) [47], ($SU(3)_F$-breaking (IRA)). (l) CLEO [55]; (m) Belle and Belle II combined. The horizontal dashed line distinguishes theoretical predictions from experimental results. The red vertical bands represent a 1σ region corresponding to the measurements. Dots with error bars represent central values with their uncertainties. Missing dots indicate no theoretical predictions or experimental results for that decay mode.

3.3. Studies of Λ_c^+ Decays

The nonleptonic weak decays of Λ_c^+ provide a unique testing ground for understanding the factorization scheme involving the $c \to s$ transition and final-state interactions. Among the possible final states, $NK^-\pi$ decays are particularly useful for examining the isospin properties of the weak interaction in Λ_c^+. In the quark-diagram scheme for $\Lambda_c^+ \to NK^-\pi$ decays, as shown in Figure 12, direct π^+ emission can proceed via a color-allowed factorizable process with external W^+ emission (Figure 12(c)), whereas a π^0 cannot be produced through this mechanism. Instead, the dominant contributions to the $NK^-\pi^0$ decays arise from color-suppressed internal W^+ emission and internal flavor conversion involving the subprocess $cd \to su$ via W^+ exchange.

The absolute branching fractions for $\Lambda_c^+ \to nK_S^0\pi^+$ and $\Lambda_c^+ \to pK_S^0\pi^0$ decays were reported by BESIII to be $\mathcal{B}(\Lambda_c^+ \to nK_S^0\pi^+) = (1.82 \pm 0.25)\%$ and $\mathcal{B}(\Lambda_c^+ \to pK_S^0\pi^0) = (1.87 \pm 0.14)\%$, respectively [56]. The branching fraction of $\Lambda_c^+ \to pK_S^0\pi^0$ relative to $\Lambda_c^+ \to pK^-\pi^+$ reported by CLEO is 0.33 ± 0.05 [57]. In 2025, the Belle II performed a precise measurement of the relative branching fraction of $\mathcal{B}(\Lambda_c^+ \to pK_S^0\pi^0)/\mathcal{B}(\Lambda_c^+ \to pK^-\pi^+)$ [13]. The invariant mass distributions of $pK^-\pi^+$ and $pK_S^0\pi^0$ for Λ_c^+ candidates are shown in Figure 13. The signal yields for $\Lambda_c^+ \to pK^-\pi^+$ and $\Lambda_c^+ \to pK_S^0\pi^0$ are $(1.405 \pm 0.003) \times 10^6$ and $(1.283 \pm 0.010) \times 10^5$, respectively. After applying a bin-by-bin correction to

 doi:10.20944/preprints202602.0472.v1

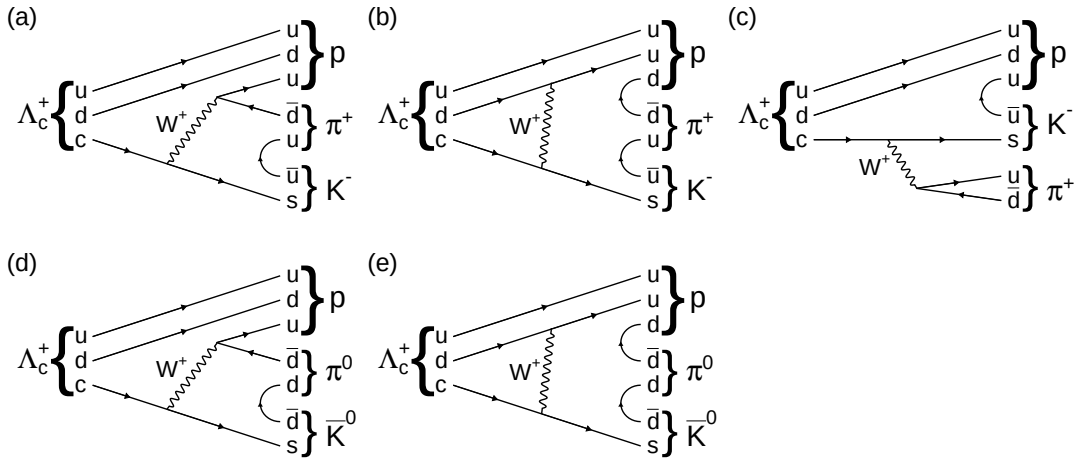

Figure 12. Typical Feynman diagrams for internal W emission (a), internal W exchange (b), and external W emission (c) processes in $\Lambda_c^+ \to pK^-\pi^+$ decays, and internal W emission (d) and internal W exchange (e) processes in $\Lambda_c^+ \to pK_S^0\pi^0$ decays.

estimate the efficiency-corrected yields of both decays, the relative branching fraction was measured to be:

$$\frac{\mathcal{B}(\Lambda_c^+ \to pK_S^0\pi^0)}{\mathcal{B}(\Lambda_c^+ \to pK^-\pi^+)} = 0.339 \pm 0.002 \pm 0.009. \tag{13}$$

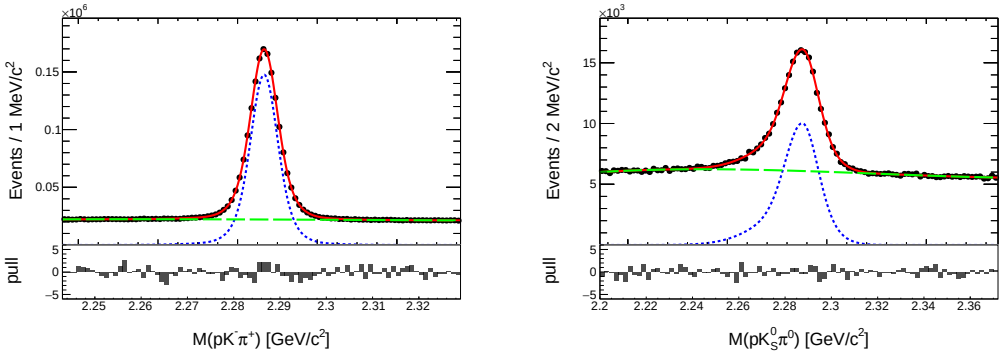

Figure 13. Invariant mass distributions of Λ_c^+ candidates and fit results for $\Lambda_c^+ \to pK^-\pi^+$ (left) and $pK_S^0\pi^0$ (right) [13]. The total fit, signal, and background are shown by solid red, dashed blue, and long dashed green curves, respectively.

By assuming that the sum of the amplitudes, $\sqrt{2}A(p\bar{K}^0\pi^0) + A(pK^-\pi^+) + A(n\bar{K}^0\pi^+)$, is zero [56,58,59], the amplitudes can be expressed in terms of two components, A_0 and A_1, corresponding to the isospin amplitudes of the $I = 0$ and $I = 1$ states of the $N\bar{K}$ system, respectively [56,58]. Defining a relative phase difference (δ) between A_0 and A_1 as $A_1/A_0 = |A_1/A_0|e^{i\delta}$, the relationship between the branching fractions and the isospin amplitudes is given by the following equations,

$$\mathcal{B}(\Lambda_c^+ \to p\bar{K}^0\pi^0) = \frac{1}{2}|A_1|^2, \tag{14}$$

$$\mathcal{B}(\Lambda_c^+ \to pK^-\pi^+) = \frac{1}{2}|A_0|^2 + \frac{1}{4}|A_1|^2 - \frac{1}{\sqrt{2}}|A_0||A_1|\cos\delta, \tag{15}$$

and

$$\mathcal{B}(\Lambda_c^+ \to n\bar{K}^0\pi^+) = \frac{1}{2}|A_0|^2 + \frac{1}{4}|A_1|^2 + \frac{1}{\sqrt{2}}|A_0||A_1|\cos\delta. \tag{16}$$

With the measured value of $\mathcal{B}(\Lambda_c^+ \to pK_S^0\pi^0)/\mathcal{B}(\Lambda_c^+ \to pK^-\pi^+)$ and the world-average $\mathcal{B}(\Lambda_c^+ \to nK_S^0\pi^+)/\mathcal{B}(\Lambda_c^+ \to pK^-\pi^+) = 0.581 \pm 0.084$ [36], $|\delta|$ was determined to be 1.842 ± 0.069,

 doi:10.20944/preprints202602.0472.v1

while the relative strength ($|A_1|/|A_0|$) was found to be 1.23 ± 0.06, where the uncertainty is the sum in quadrature of the statistical uncertainty and the uncertainty in $\mathcal{B}(\Lambda_c^+ \to nK_S^0\pi^+)/\mathcal{B}(\Lambda_c^+ \to pK^-\pi^+)$. The results show that the isospin amplitude A_1 is not significantly suppressed compared to A_0 in Λ_c^+ decays. Here, we note that the calculation assumes isospin symmetry for the non-resonant contributions [58].

In addition, Belle II carried out the first study of intermediate resonant contributions in the decay $\Lambda_c^+ \to pK_S^0\pi^0$ [13]. Figure 14 presents the Dalitz distribution of $M^2(K_S^0\pi^0)$ versus $M^2(pK_S^0)$ for the decay $\Lambda_c^+ \to pK_S^0\pi^0$, where several enhanced regions associated with intermediate resonant contributions are visible. To study these intermediate states in more detail, the Dalitz plot is projected onto the one-dimensional invariant mass spectra of $M(pK_S^0)$, $M(K_S^0\pi^0)$, and $M(p\pi^0)$. The spectra are corrected for reconstruction efficiency, and the non-Λ_c^+ background is subtracted by fitting the reconstructed Λ_c^+ mass distribution in each bin. In the $M(pK_S^0)$ spectrum and the Dalitz plot of the $\Lambda_c^+ \to pK_S^0\pi^0$ decay, shown in Figure 15(a) and on the left panel of Figure 14, respectively, Σ^* hyperon contributions are found to be relatively weak. Nevertheless, clear localized structures appear in the $M(pK^-)$ distribution, which can be tentatively interpreted as the $\Lambda(1520)$ and $\Lambda(1670)$ resonances, as illustrated in Figure 15(b). This observation is consistent with the expectation that Λ^* hyperons are favored over Σ^* states in the π^+ emission processes [36]. Such a hierarchy may be understood as a consequence of the production mechanism in the $\Lambda_c^+ \to pK_S^0\pi^0$ decay being dominated by color-suppressed, factorized transitions.

The contribution associated with the $\Delta(1232)$ resonance is found to be significantly weaker in the $M(p\pi^0)$ spectrum of the $\Lambda_c^+ \to pK_S^0\pi^0$ channel (Figure 15(c)) than in the $M(p\pi^+)$ distribution observed in the $\Lambda_c^+ \to pK^-\pi^+$ channel (Figure 15(d)). This reduction can be understood as a consequence of isospin symmetry, which favors the $\Delta^{++}K^-$ production channel over the Δ^+K^0 channel. In addition, a pronounced enhancement close to the $p\eta$ mass threshold is present in the $M(p\pi^0)$ spectrum of the $\Lambda_c^+ \to pK_S^0\pi^0$ decay. This structure corresponds to the diagonal feature observed in the Dalitz distribution shown on the left side of Figure 14. A similar enhancement was previously reported in the study of $\Lambda_c^+ \to pK_S^0\eta$ decays [60]. The resemblance between this structure and the $\Lambda\eta$ threshold cusp, which is enhanced by the $\Lambda(1670)$ resonance in the pK^- system (Figure 15(b)) [61,62], suggests that the feature near the $p\eta$ threshold in Figure 15(c) may originate from a threshold cusp amplified by the $N(1535)^+$ state.

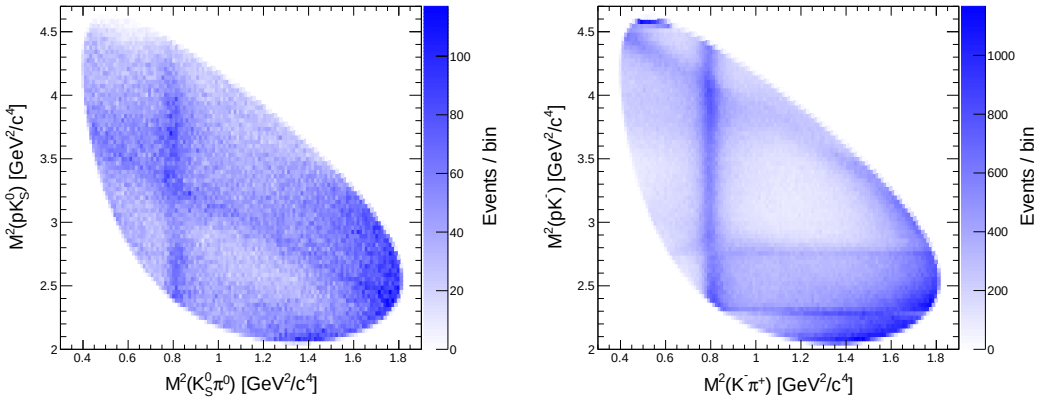

Figure 14. Dalitz distributions for the decays $\Lambda_c^+ \to pK_S^0\pi^0$ (left) and $\Lambda_c^+ \to pK^-\pi^+$ (right), selected within the invariant mass windows $2.263\ \text{GeV}/c^2 < M(pK_S^0\pi^0) < 2.306\ \text{GeV}/c^2$ and $2.274\ \text{GeV}/c^2 < M(pK^-\pi^+) < 2.298\ \text{GeV}/c^2$, respectively [13]. The bin sizes along both Dalitz axes are set to $0.02\ \text{GeV}^2/c^4$. Non-Λ_c^+ background contributions are retained in the displayed Dalitz plots.

Preprints.org (www.preprints.org) | NOT PEER-REVIEWED | Posted: 6 February 2026 doi:10.20944/preprints202602.0472.v1

Both $\Lambda_c^+ \to pK^-\pi^+$ and $\Lambda_c^+ \to pK_S^0\pi^0$ decays also exhibit a distinct signal associated with the vector meson $K^*(892)^0$, as illustrated in Figure 15(e) and (f). In the higher-mass region of the K^* system, an enhancement beyond phase-space expectations is observed in both decay modes. To further clarify the role of isospin symmetry in Λ_c^+ decays and to improve the understanding of intermediate resonant contributions, such as Λ^*, Σ^*, Δ^*, and N^* states, a dedicated amplitude analysis employing the helicity formalism for these two channels is suggested.

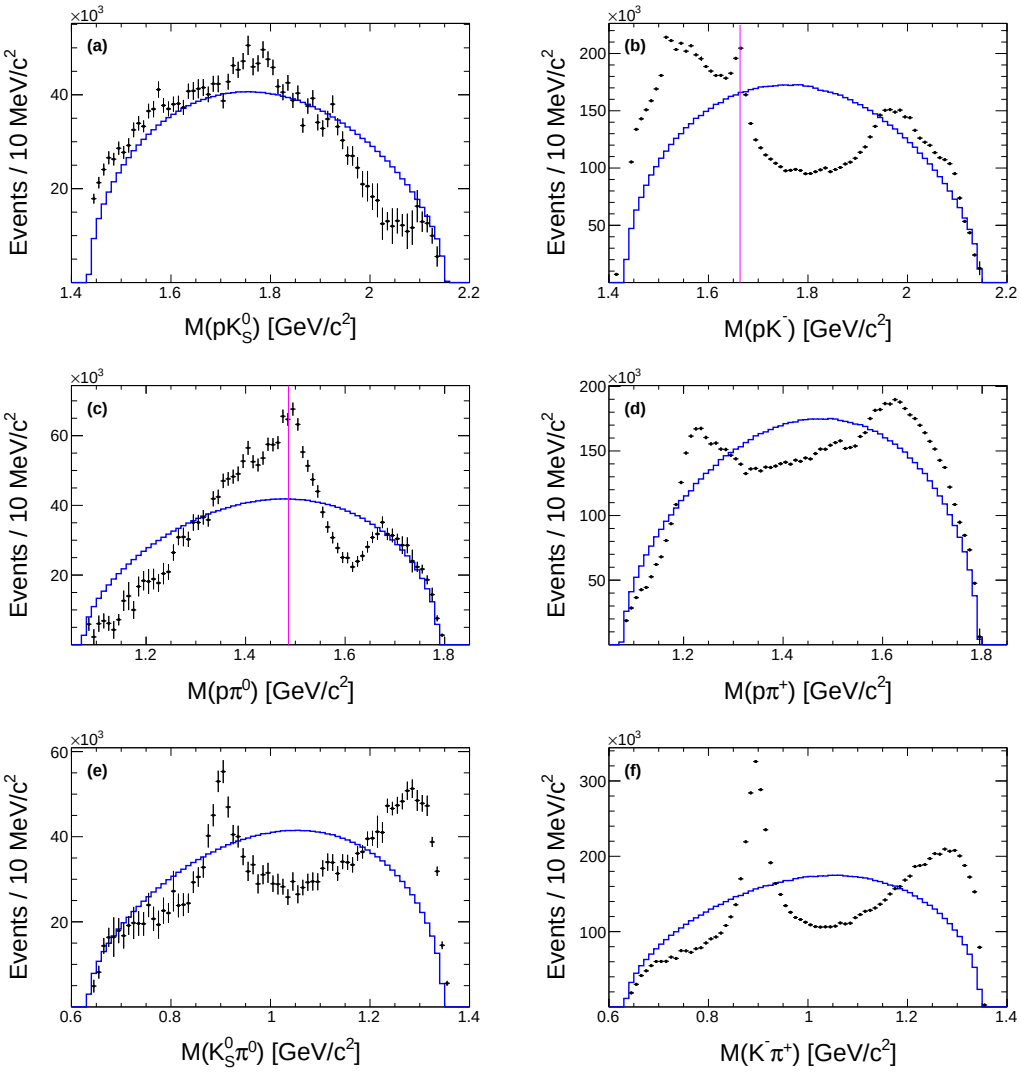

Figure 15. invariant mass projection spectra for the decays $\Lambda_c^+ \to pK_S^0\pi^0$ (left) and $\Lambda_c^+ \to pK^-\pi^+$ (right) after subtraction of background contributions and correction for reconstruction efficiency [13]. The expectations from signal Monte Carlo simulations generated according to a phase-space model are overlaid and shown as blue histograms. A pronounced enhancement close to the $p\eta$ mass threshold is observed in panel (c), while the $\Lambda\eta$ and $p\eta$ thresholds are indicated in panels (b) and (c), respectively. In addition, a distinct resonance peak corresponding to the K^* is visible in the $K_S^0\pi^0$ invariant mass distribution shown in panels (e) and (f).

4. Branching Fractions of Charmed Baryons in B Meson Decays

Baryonic B decays provide a valuable laboratory for investigating the production mechanisms of baryon–antibaryon pairs in the nonperturbative regime of QCD. Over the past three decades, a variety of baryonic B decay modes have been observed [36], exhibiting several remarkable features, including threshold enhancements in the baryon–antibaryon invariant mass spectra [63–66] and a pronounced hierarchy between two-body and multi-body branching fractions [67,68]. These phenomena offer important insights into the kinematic structure and dynamical properties governing baryonic B decays [69].

 doi:10.20944/preprints202602.0472.v1

In 2003, Belle reported the first observation of a two-body baryonic B decay and measured the branching fraction of $B^0 \to \Lambda_c^- p$ to be of order 10^{-5} [70]. Subsequently, in 2006, Belle observed the doubly charmed decay $B \to \Lambda_c^+ \Xi_c$ [71], which was later confirmed by BaBar [72]. In contrast to singly charmed modes, these doubly charmed baryonic B decays were found to have branching fractions at the level of 10^{-3}. The decay processes $B^0 \to \Lambda_c^- p$ and $B \to \Lambda_c^+ \Xi_c$ are governed by the quark-level transitions $b \to c\bar{u}d$ and $b \to c\bar{c}s$, respectively, and involve Cabibbo–Kobayashi–Maskawa (CKM) matrix elements of comparable magnitudes [73]. Nevertheless, their branching fractions differ by nearly two orders of magnitude, indicating that additional dynamical mechanisms may strongly enhance or suppress specific decay channels.

A number of theoretical explanations have been proposed to account for the large decay rates into charmed baryon pairs, including soft nonperturbative mechanisms such as σ/π meson exchange [74, 75], final-state interactions [76], and hard-gluon exchange contributions [77]. Further experimental studies of baryonic B decays into charmed baryon pairs therefore provide crucial input for probing the underlying decay dynamics and for discriminating among competing theoretical interpretations.

From the theoretical perspective, the decays $B^+ \to \Sigma_c(2455)^{++}\bar{\Xi}_c^-$ and $B^0 \to \Sigma_c(2455)^0\bar{\Xi}_c^0$ have been investigated using both the QCD sum rule approach [78] and the diquark model [79]. The QCD sum rule calculations predict branching fractions as large as 4×10^{-3} [78], while the diquark model estimates values of order 10^{-4}, corresponding to roughly 30%–70% of those for the $B^+ \to \Lambda_c^+ \bar{\Xi}_c^0$ and $B^0 \to \Lambda_c^+ \Xi_c^-$ decay modes [79]. These processes proceed via purely internal W-boson emission [80], as illustrated in Figure 16, which generates nonfactorizable amplitudes [81] arising from nonperturbative QCD effects such as final-state interactions and soft-gluon exchanges [82–85].

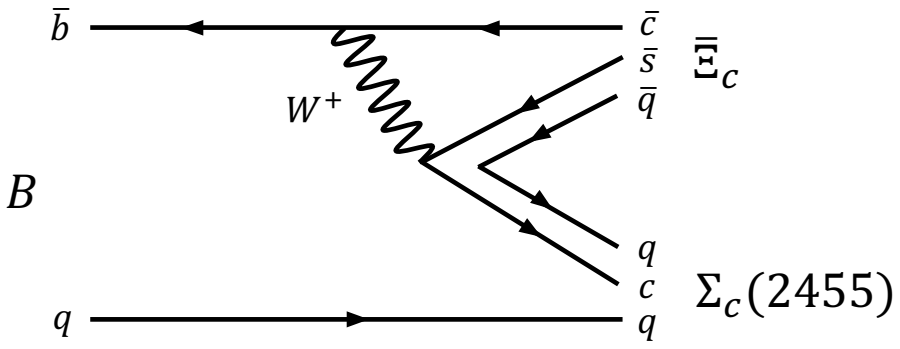

Figure 16. Diagram representing the internal W-boson emission amplitude for the decays $B^+ \to \Sigma_c(2455)^{++}\bar{\Xi}_c^-$ and $B^0 \to \Sigma_c(2455)^0\bar{\Xi}_c^0$, corresponding to $q = u$ and $q = d$, respectively.

Within the framework of SU(3) flavor symmetry, the $\Sigma_c(2455)$ baryon belongs to a sextet representation of flavor-symmetric states, whereas the Ξ_c baryon is classified as a member of the antitriplet of flavor-antisymmetric states. To date, no B decays into charmed baryon pairs involving both a sextet and an antitriplet have been experimentally observed.

In 2025, Belle II reported the first observation of the two-body baryonic decays $B^+ \to \Sigma_c(2455)^{++}\bar{\Xi}_c^-$ and $B^0 \to \Sigma_c(2455)^0\bar{\Xi}_c^0$, using e^+e^- collision data samples containing 772×10^6 and 387×10^6 $B\bar{B}$ events collected by the Belle and Belle II detectors, respectively [14]. The yields are extracted from a two-dimensional fit to the distributions of the difference between the expected and observed B-meson energy (ΔE) and the $\Lambda_c^+\pi$ invariant mass. The fit results are shown in Figure 17. Fits to data combining Belle and Belle II samples yield 52.8 ± 10.2 and 31.1 ± 7.2 signal events for the $B^+ \to \Sigma_c(2455)^{++}\bar{\Xi}_c^-$ and $B^0 \to \Sigma_c(2455)^0\bar{\Xi}_c^0$ decay modes, corresponding to statistical significances of 7.3σ and 6.2σ, respectively. The branching fractions were measured to be

$$\mathcal{B}(B^+ \to \Sigma_c(2455)^{++}\,\bar{\Xi}_c^-) = \left(5.74 \pm 1.11 \pm 0.42^{+2.47}_{-1.53}\right) \times 10^{-4} \tag{17}$$

 doi:10.20944/preprints202602.0472.v1

and

$$\mathcal{B}\Big(B^0 \to \Sigma_c(2455)^0\,\bar{\Xi}_c^0\Big) = \Big(4.83 \pm 1.12 \pm 0.37^{+0.72}_{-0.60}\Big) \times 10^{-4}. \tag{18}$$

The first and second uncertainties are statistical and systematic, respectively, while the third ones arise from the absolute branching fractions of $\bar{\Xi}_c^-$ or $\bar{\Xi}_c^0$ decays. The observed branching fractions are one order of magnitude smaller than those predicted by the QCD sum rule [78], but are consistent with the expectations of the diquark model [79]. Interestingly, these branching fractions are larger than those of their singly charmed counterparts, $B^+ \to \Sigma_c(2455)^{++}\bar{p}$ and $B^0 \to \Sigma_c(2455)^0\bar{p}$, by about two orders of magnitude [36], although the corresponding combinations of CKM matrix elements in their amplitudes have nearly equal magnitudes.

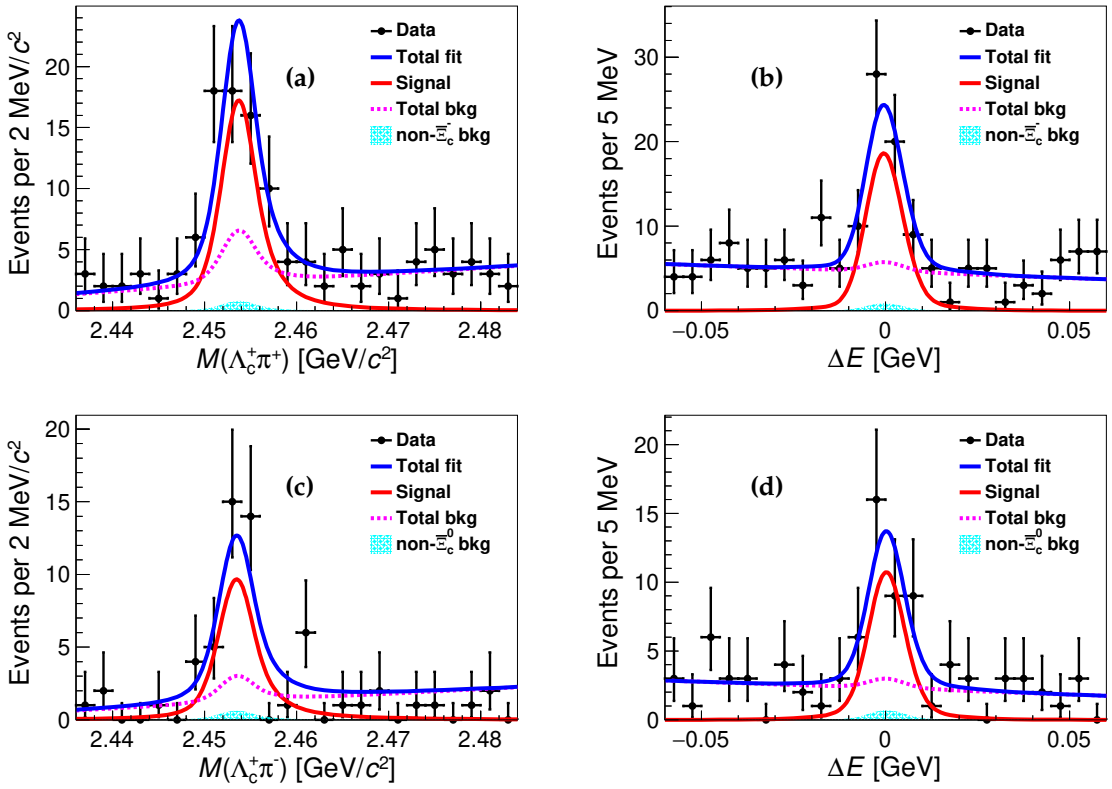

Figure 17. Distributions of (a,c) $M(\Lambda_c^+\pi^\pm)$ and (b,d) ΔE for the reconstructed (top) $B^+ \to \Sigma_c(2455)^{++}\bar{\Xi}_c^-$ and (bottom) $B^0 \to \Sigma_c(2455)^0\bar{\Xi}_c^0$ candidates, using events from the signal regions of $M(\bar{\Xi}_c^{-,0})$ in the combined Belle and Belle II data sets [14]. Points with error bars represent the data, the solid blue curves show the total fit results, the solid red curves correspond to the fitted signal components, and the dashed magenta curves represent the total fitted background components. The shaded cyan regions indicate the peaking-background contributions from the inclusive $B^{+,0} \to \Sigma_c(2455)^{++,0}X$ decays, where $X \neq \bar{\Xi}_c^{-,0}$.

5. Asymmetry Parameter

In addition to the branching fraction measurement, parity violation in Ξ_c^0 decays can be measured using the decay asymmetry parameter α. In the case of the $\Xi_c^0 \to \Xi^0\pi^0$ decay, α can be extracted by fitting the Ξ_c^0 decay angular distribution according to the differential decay rate function

$$\frac{dN}{d\cos\theta_{\Xi^0}} \propto 1 + \alpha(\Xi_c^0 \to \Xi^0\pi^0)\,\alpha(\Xi^0 \to \Lambda\pi^0)\cos\theta_{\Xi^0}, \tag{19}$$

where $\alpha(\Xi^0 \to \Lambda\pi^0)$ is the decay asymmetry parameter of the $\Xi^0 \to \Lambda\pi^0$ decay, and $\cos\theta_{\Xi^0}$ is defined as the cosine of the angle between the Λ momentum vector and the opposite of the Ξ_c^0 momentum vector in the Ξ^0 rest frame. In weak decays, the interference between parity-violating and parity-conserving amplitudes gives rise to an asymmetry in the angular distribution, which can be quantified

 doi:10.20944/preprints202602.0472.v1

by the parameter α. The decay asymmetry parameter for the process $\Xi_c^0 \to \Xi^0\pi^0$ has been investigated in a number of theoretical models, as summarized in Figure 4. The predicted values differ significantly among different models. Therefore, an experimental determination of the decay asymmetry parameter for this channel is highly desirable.

In 2024, the Belle II presented the first measurement of the decay asymmetry parameter for the decay $\Xi_c^0 \to \Xi^0\pi^0$ [9]. The final Ξ_c^0 signal yields in bins of $\cos\theta_{\Xi^0}$ for $\Xi_c^0 \to \Xi^0\pi^0$ are shown in Figure 18, together with the results of the simultaneous fit using Eq. (19) with the common $\alpha(\Xi_c^0 \to \Xi^0 h^0)\,\alpha(\Xi^0 \to \Lambda\pi^0)$ for the Belle and Belle II data samples. Using simulated pseudo-experiments generated with different values of α, Belle and Belle II test the α extraction procedure and finds that it is linear. The product of asymmetry parameters is obtained to be

$$\alpha(\Xi_c^0 \to \Xi^0\pi^0)\,\alpha(\Xi^0 \to \Lambda\pi^0) = 0.32 \pm 0.05\,(\text{stat.}). \tag{20}$$

Taking $\alpha(\Xi^0 \to \Lambda\pi^0) = -0.349 \pm 0.009$ [36], the value of $\alpha(\Xi_c^0 \to \Xi^0\pi^0)$ is calculated to be $-0.90 \pm 0.15\,(\text{stat.}) \pm 0.23\,(\text{syst.})$. The values of $\alpha(\Xi_c^0 \to \Xi^0\pi^0)$ extracted via individual fits to the Belle and Belle II data samples are -0.84 ± 0.21 and -0.98 ± 0.22, respectively, where the uncertainties are statistical only. These results are in good agreement with that obtained from the simultaneous fit.

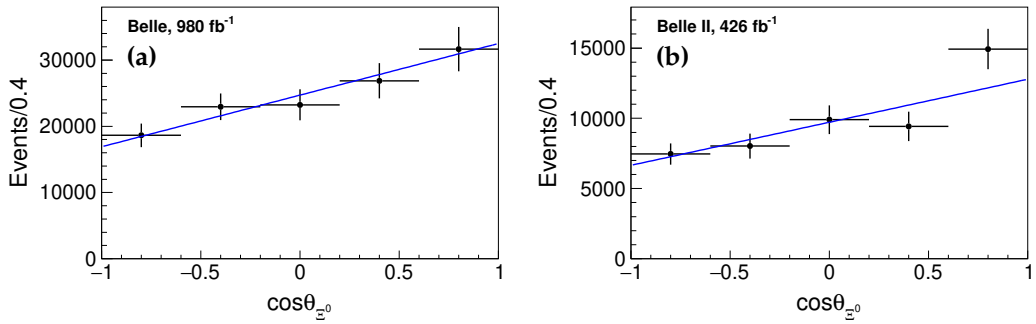

Figure 18. The Ξ_c^0 signal yields in bins of $\cos\theta_{\Xi^0}$ from the (a) Belle and (b) Belle II datasets [9]. The lines show the linear regression results.

6. CP Violation

A viable way to investigate CP violation and examine U-spin symmetry is to study SCS three-body hadronic decays of charmed baryons [26,27]. Under the assumption of exact U-spin symmetry, the following relations hold:

$$A_{CP}(\Xi_c^+ \to \Sigma^+\pi^+\pi^-) + A_{CP}(\Lambda_c^+ \to pK^+K^-) = 0, \tag{21}$$
$$A_{CP}(\Xi_c^+ \to \Sigma^+K^+K^-) + A_{CP}(\Lambda_c^+ \to p\pi^+\pi^-) = 0. \tag{22}$$

Despite the large branching fractions of these decay modes, none of the individual CP asymmetries, nor their U-spin sums, have been experimentally determined so far. LHCb has measured the difference between $A_{CP}(\Lambda_c^+ \to pK^+K^-)$ and $A_{CP}(\Lambda_c^+ \to p\pi^+\pi^-)$ [86]; however, since these two modes are not connected by U-spin symmetry, this result does not provide direct information on U-spin-symmetry breaking.

In 2025, Belle II presented the first measurements of the CP asymmetries in the decays $\Xi_c^+ \to \Sigma^+h^+h^-$ and $\Lambda_c^+ \to ph^+h^-$, where h denotes either a kaon or a pion [28]. The analysis is based on Belle II data sample corresponding to an integrated luminosity of 428 fb^{-1} of e^+e^- collisions, collected by the Belle II experiment at or near the $\Upsilon(4S)$ C.M. energy between 2019 and 2022.

The CP asymmetry in the decay rate of a charmed baryon X_c^+ into a final state f^+ is defined as

$$A_{CP}(X_c^+ \to f^+) \equiv \frac{\Gamma(X_c^+ \to f^+) - \Gamma(\bar{X}_c^- \to \bar{f}^-)}{\Gamma(X_c^+ \to f^+) + \Gamma(\bar{X}_c^- \to \bar{f}^-)}. \tag{23}$$

 doi:10.20944/preprints202602.0472.v1

Experimentally, this quantity is obtained from the asymmetry in the reconstructed signal yields,

$$A_N(X_c^+ \to f^+) \equiv \frac{N(X_c^+ \to f^+) - N(\bar{X}_c^- \to \bar{f}^-)}{N(X_c^+ \to f^+) + N(\bar{X}_c^- \to \bar{f}^-)}, \tag{24}$$

after applying corrections for detector-induced and production-related asymmetries. For sufficiently small asymmetries, one can express A_N as

$$A_N(X_c^+ \to f^+) = A_{CP}(X_c^+ \to f^+) + A_P(X_c^+) + A_d(f^+), \tag{25}$$

where $A_P(X_c^+)$ accounts for the forward–backward asymmetry in charmed baryon production in e^+e^- collisions [87–89], and $A_d(f^+)$ denotes the detection asymmetry associated with the charged final-state particles. Since the production asymmetry A_P is an odd function of the cosine of the polar angle of the charmed baryon momentum in the e^+e^- C.M. frame, $\cos\theta$, its contribution can be suppressed by replacing the raw yield asymmetry A_N in Eq. (24) with the average value measured in the forward and backward hemispheres,

$$A'_N = \frac{A_N(\cos\theta > 0) + A_N(\cos\theta < 0)}{2}. \tag{26}$$

The detection asymmetries associated with charged particles are removed by subtracting the yield asymmetries measured in several CF control channels, including $\Lambda_c^+ \to \Sigma^+ h^+ h^-$, $\Lambda_c^+ \to p\pi^+K^-$, and $D^0 \to \pi^+K^-\pi^+\pi^-$. The decay mode $D^0 \to \pi^+K^-\pi^+\pi^-$ is chosen instead of $D^0 \to \pi^+K^-$ because the phase-space distributions of the $K^-\pi^+$ pair in the former are similar to those in $\Lambda_c^+ \to p\pi^+K^-$, while this similarity does not hold for $D^0 \to \pi^+K^-$. As these control channels are Cabibbo favored, they are expected to have negligible CP asymmetries, which are therefore assumed to be zero.

The decay-rate CP asymmetry for the process $\Xi_c^+ \to \Sigma^+ h^+ h^-$ is determined as

$$A_{CP}(\Xi_c^+ \to \Sigma^+ h^+ h^-) = A'_N(\Xi_c^+ \to \Sigma^+ h^+ h^-) - A'_N(\Lambda_c^+ \to \Sigma^+ h^+ h^-), \tag{27}$$

while that for $\Lambda_c^+ \to p h^+ h^-$ is given by

$$A_{CP}(\Lambda_c^+ \to p h^+ h^-) = A'_N(\Lambda_c^+ \to p h^+ h^-) - A'_N(\Lambda_c^+ \to p\pi^+K^-) + A'_N(D^0 \to \pi^+K^-\pi^+\pi^-). \tag{28}$$

In this procedure, subtracting the Λ_c^+ asymmetries cancels the detection asymmetries associated with the final-state baryon, while including the D^0 term eliminates the residual detection asymmetries of the K^- and π^+ introduced by the subtraction of $A'_N(\Lambda_c^+ \to p\pi^+K^-)$. For the control channels, the distributions of the charmed baryon momentum in the C.M. frame and of $\cos\theta$ are required to match those of the signal channels. In addition, the kinematic distributions of the kaon–pion pair are aligned by applying event-by-event kinematic weights.

Figures 19 and 20 show the mass distributions of the candidates for each decay channel, the results of the final fit, and the resulting averaged yield asymmetries as functions of the masses. Table 3 lists the measured yields and forward, backward, and averaged yield asymmetries.

 doi:10.20944/preprints202602.0472.v1

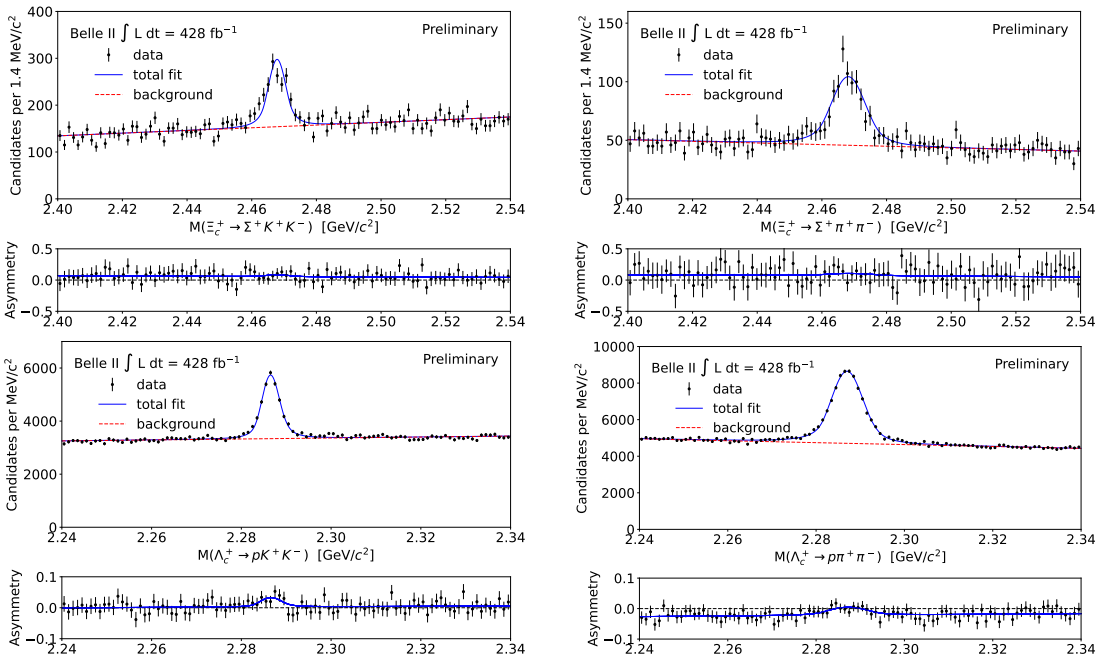

Figure 19. Mass distributions for $\Xi_c^+ \to \Sigma^+ h^+ h^-$ (top) and $\Lambda_c^+ \to p h^+ h^-$ (bottom) candidates for $h = K$ (left) and π (right), together with the results of the fits, summing forward and backward contributions, and their averaged yield asymmetries as functions of mass, with the fit projections overlaid [28].

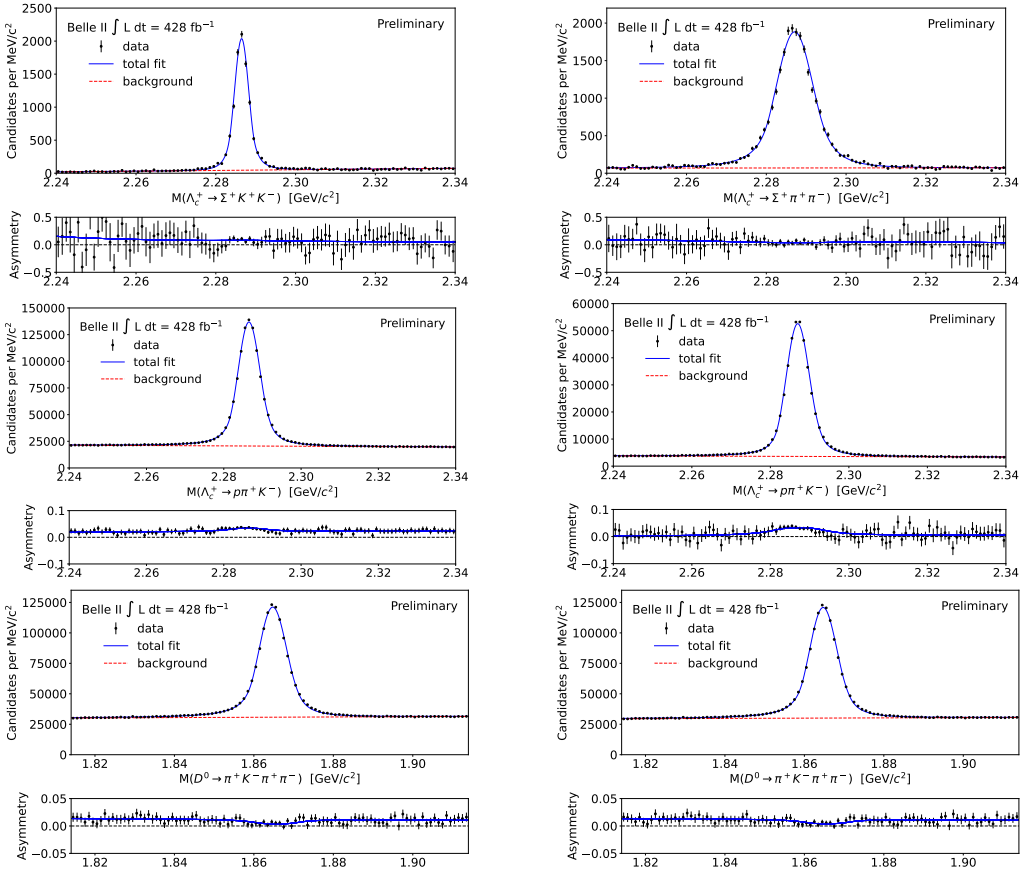

Figure 20. Mass distributions for $\Lambda_c^+ \to \Sigma^+ h^+ h^-$ (top), $\Lambda_c^+ \to p\pi^+ K^-$ (middle), and $D^0 \to \pi^+ K^- \pi^+ \pi^-$ (bottom) candidates, using the selection criteria for $\Lambda_c^+ \to p K^+ K^-$ (left) and $\Lambda_c^+ \to p\pi^+\pi^-$ (right), together with the results of the fits, summing forward and backward contributions, and their averaged yield asymmetries as functions of mass, with the fit projections overlaid [28].

 doi:10.20944/preprints202602.0472.v1

Table 3. Yields (in 10^3) and asymmetries (in %) with statistical uncertainties [28]. † and ‡ indicate candidates selected and kinematically weighted for the $\Lambda_c^+ \to pK^+K^-$ and $\Lambda_c^+ \to p\pi^+\pi^-$ modes, respectively.

Decay mode	Yield	Forward A_N	Backward A_N	A'_N
$\Xi_c^+ \to \Sigma^+K^+K^-$	0.78 ± 0.05	13.0 ± 9.2	10.5 ± 9.2	11.7 ± 6.5
$\Lambda_c^+ \to \Sigma^+K^+K^-$	9.9 ± 0.1	10.9 ± 1.5	5.3 ± 1.6	8.1 ± 1.1
$\Xi_c^+ \to \Sigma^+\pi^+\pi^-$	0.62 ± 0.04	17.0 ± 10.0	9.7 ± 8.9	13.3 ± 6.8
$\Lambda_c^+ \to \Sigma^+\pi^+\pi^-$	23.4 ± 0.2	7.4 ± 1.0	0.2 ± 1.0	3.8 ± 0.8
$\Lambda_c^+ \to pK^+K^-$	13.6 ± 0.2	9.3 ± 2.2	5.5 ± 2.4	7.4 ± 1.7
† $\Lambda_c^+ \to p\pi^+K^-$	955.0 ± 1.3	5.6 ± 0.2	1.6 ± 0.2	3.6 ± 0.1
† $D^0 \to \pi^+K^-\pi^+\pi^-$	928.0 ± 1.4	1.6 ± 0.2	-1.5 ± 0.2	0.1 ± 0.2
$\Lambda_c^+ \to p\pi^+\pi^-$	40.5 ± 0.4	5.8 ± 1.3	1.5 ± 1.4	3.6 ± 0.9
‡ $\Lambda_c^+ \to p\pi^+K^-$	410.3 ± 0.7	5.4 ± 0.3	1.5 ± 0.3	3.4 ± 0.2
‡ $D^0 \to \pi^+K^-\pi^+\pi^-$	925.2 ± 1.4	1.6 ± 0.2	-1.3 ± 0.2	0.1 ± 0.2

Using 428 fb^{-1} of e^+e^- collisions collected by Belle II, Belle II measured

$$A_{CP}(\Xi_c^+ \to \Sigma^+K^+K^-) = (3.7 \pm 6.6 \pm 0.6)\%, \quad (29)$$
$$A_{CP}(\Xi_c^+ \to \Sigma^+\pi^+\pi^-) = (9.5 \pm 6.8 \pm 0.5)\%, \quad (30)$$
$$A_{CP}(\Lambda_c^+ \to pK^+K^-) = (3.9 \pm 1.7 \pm 0.7)\%, \quad (31)$$
$$A_{CP}(\Lambda_c^+ \to p\pi^+\pi^-) = (0.3 \pm 1.0 \pm 0.2)\%. \quad (32)$$

These results are consistent with CP symmetry. Their U-spin sums are

$$A_{CP}(\Xi_c^+ \to \Sigma^+\pi^+\pi^-) + A_{CP}(\Lambda_c^+ \to pK^+K^-) = (13.4 \pm 7.0 \pm 0.9)\%, \quad (33)$$
$$A_{CP}(\Xi_c^+ \to \Sigma^+K^+K^-) + A_{CP}(\Lambda_c^+ \to p\pi^+\pi^-) = (4.0 \pm 6.6 \pm 0.7)\%, \quad (34)$$

which are consistent with U-spin symmetry.

These are the world's first measurements of A_{CP} for individual hadronic three-body charmed baryon decays. The uncertainties are dominated by statistical contributions; therefore, future measurements with larger data samples collected by Belle II will enable us to perform precision searches for CP violation and to carry out stringent tests of U-spin sum rules.

7. Summary and Outlook

We summarize the recent experimental progress on charmed baryons achieved by the Belle and Belle II experiments. Several absolute branching fractions for Λ_c^+, Ξ_c^+, and Ξ_c^0 decays have been determined for the first time or with the highest precision, as presented in Table 2. The decays $B^+ \to \Sigma_c(2455)^{++}\bar{\Xi}_c^-$ and $B^0 \to \Sigma_c(2455)^0\bar{\Xi}_c^0$ have been found. The corresponding branching fractions were measured to be $\mathcal{B}(B^+ \to \Sigma_c(2455)^{++}\bar{\Xi}_c^-) = (5.74 \pm 2.74) \times 10^{-4}$ and $\mathcal{B}(B^0 \to \Sigma_c(2455)^0\bar{\Xi}_c^0) = (4.83 \pm 1.38) \times 10^{-4}$. The asymmetry parameter for $\Xi_c^0 \to \Xi^0\pi^0$ was obtained to be -0.90 ± 0.27. No CP asymmetries in the SCS decays $\Xi_c^+ \to \Sigma^+K^+K^-$, $\Xi_c^+ \to \Sigma^+\pi^+\pi^-$, $\Lambda_c^+ \to pK^+K^-$, and $\Lambda_c^+ \to p\pi^+\pi^-$were found. The U-spin symmetry was measured to be consistent with zero. The first-time and updated measurements of the branching fraction and asymmetry parameter serve as essential inputs for flavor-symmetry analyses and dynamical models. The first Belle II measurements of CP violation in three-body SCS decays of Ξ_c^+ and Λ_c^+ open a new avenue for quantitative tests of U-spin relations and for searching for effects beyond SM expectations.

The Belle II experiment, operating at a high-luminosity electron–positron collider, offers an excellent platform characterized by low background levels and well-identified final states. Benefiting from improved vertex reconstruction performance, long-lived particles such as Λ, Ξ, Λ_c, and Ξ_c can be detected with higher efficiency at Belle II. The total integrated luminosity at Belle and Belle II exceeds 1.6 ab^{-1}. The integrated luminosity at Belle II is expected to achieve 4 ab^{-1} and 10 ab^{-1} in 2029 and

 doi:10.20944/preprints202602.0472.v1

2034, respectively [90]. Therefore, using large data samples, Belle II will substantially improve the accuracy of measurements of branching fraction, decay asymmetry, and CP violation, and extend such studies to a wider set of channels. These forthcoming high-statistics results are expected to sharpen discrimination among competing theoretical frameworks and to stimulate sustained progress in understanding the nonleptonic weak dynamics of charmed baryons.

Author Contributions: Conceptualization, S.J and C.-P.S; investigation, Y.-W.Z and S.J; writing—original draft preparation, Y.-W.Z; writing—review and editing, Y.-W.Z, S.J, and C.-P.S; supervision, S.J and C.-P.S. All authors have read and agreed to the published version of the manuscript.

Funding: This work is supported by National Key R&D Program of China under contract Nos. 2024YFA1610503, and 2024YFA1610504. National Natural Science Foundation of China under contract Nos. 121350051419 and 12475076; Fundamental Research Funds of China for the Central Universities under contract Nos. 2242025RCB00141420 and RF1028623046.

Institutional Review Board Statement: Not applicable.

Informed Consent Statement: Not applicable.

Data Availability Statement: Not applicable.

Conflicts of Interest: The authors declare no conflict of interest.

Abbreviations

The following abbreviations are used in this manuscript:

CPV	CP Violation
CF	Cabibbo–Favored
CS	Cabibbo–Suppressed
SCS	singly Cabibbo–Suppressed
SM	Standard Model

References

1. J. F. Donoghue and S. Pakvasa, *Signals of CP Nonconservation in Hyperon Decay*, Phys. Rev. Lett. **55**, 162 (1985). [CrossRef]
2. A. D. Sakharov, *Violation of CP Invariance, C Asymmetry, and Baryon Asymmetry of the Universe*, Pisma Zh. Eksp. Teor. Fiz. **5**, 32–35 (1967). [CrossRef]
3. L. L. Chau, H. Y. Cheng, and B. Tseng, *Analysis of two-body decays of charmed baryons using the quark-diagram scheme*, Phys. Rev. D **54**, 2132 (1996). [CrossRef]
4. H. Y. Cheng, *Charmed baryons circa 2015*, Front. Phys. **10**, 101406 (2015). [CrossRef]
5. H. Y. Cheng, *Charmed baryon physics circa 2021*, Chin. J. Phys. **78**, 324 (2022). [CrossRef]
6. A. Zupanc *et al.* (Belle Collaboration), *Measurement of the Branching Fraction of* $\Lambda_c^+ \to pK^-\pi^+$, Phys. Rev. Lett. **113**, 042002 (2014). [CrossRef]
7. Y. B. Li *et al.* (Belle Collaboration), *First Measurements of Absolute Branching Fractions of the* Ξ_c^0 *Baryon at Belle*, Phys. Rev. Lett. **122**, 082001 (2019). [CrossRef]
8. Y. B. Li *et al.* (Belle Collaboration), *First Measurements of Absolute Branching Fractions of the* Ξ_c^+ *Baryon at Belle*, Phys. Rev. D **100**, 031101 (2019). [CrossRef]
9. I. Adachi *et al.* (Belle and Belle II Collaborations), *Measurements of the branching fractions of* $\Xi_c^0 \to \Xi^0\pi^0$, $\Xi_c^0 \to \Xi^0\eta$, *and* $\Xi_c^0 \to \Xi^0\eta'$ *and the decay asymmetry parameter of* $\Xi_c^0 \to \Xi^0\pi^0$, JHEP **10**, 045 (2024). [CrossRef]
10. M. Abumusabh *et al.* (Belle and Belle II Collaborations), *First measurements of the branching fractions for the decay modes* $\Xi_c^0 \to \Lambda\eta$ *and* $\Xi_c^0 \to \Lambda\eta'$ *and search for the decay* $\Xi_c^0 \to \Lambda\pi^0$ *using Belle and Belle II data*, JHEP **03**, 061 (2025). [CrossRef]
11. I. Adachi *et al.* (Belle and Belle II Collaborations), *Observations of the singly Cabibbo-suppressed decays* $\Xi_c^+ \to pK_S^0$, $\Xi_c^+ \to \Lambda\pi^+$, *and* $\Xi_c^+ \to \Sigma^0\pi^+$ *at Belle and Belle II*, JHEP **03**, 061 (2025). [CrossRef]
12. I. Adachi *et al.* (Belle and Belle II Collaborations), *Measurements of the branching fractions of* $\Xi_c^+ \to \Sigma^+K_S^0$, $\Xi_c^+ \to \Xi^0\pi^+$, *and* $\Xi_c^+ \to \Xi^0K^+$ *at Belle and Belle II*, JHEP **08**, 195 (2025). [CrossRef]

 doi:10.20944/preprints202602.0472.v1

13. I. Adachi *et al.* (Belle and Belle II Collaborations), *Measurement of the branching fraction of $\Lambda_c^+ \to pK_S^0\pi^0$ at Belle*, Phys. Rev. D **112**, 092005 (2025). [CrossRef]
14. M. Abumusabh *et al.* (Belle and Belle II Collaborations), *Observation of the decays $B^+ \to \Sigma_c(2455)^{++}\,\bar{\Xi}_c^-$ and $B^0 \to \Sigma_c(2455)^0\,\bar{\Xi}_c^0$*, Phys. Rev. D **112**, 052001 (2025). [CrossRef]
15. T. D. Lee and C. N. Yang, *General partial wave analysis of the decay of a hyperon of spin 1/2*, Phys. Rev. **108**, 1645–1647 (1957). [CrossRef]
16. A. D. Sakharov, *Baryon asymmetry of the universe*, Sov. Phys. Usp. **34**, 65–80 (1990). [CrossRef]
17. M. E. Shaposhnikov, *Baryon asymmetry of the Universe in Standard Electroweak Theory*, Nucl. Phys. B **287**, 757–775 (1987). [CrossRef]
18. R. Aaij *et al.* (LHCb Collaboration), *Observation of charge–parity symmetry breaking in baryon decays*, Nature **643**, 1223–1228 (2025). [CrossRef]
19. J. Brod, A. L. Kagan, and J. Zupan, *Size of direct CP violation in singly Cabibbo-suppressed D decays*, Phys. Rev. D **86**, 014023 (2012). [CrossRef]
20. H. Y. Cheng and C. W. Chiang, *Direct CP violation in two-body hadronic charmed meson decays*, Phys. Rev. D **85**, 034036 (2012); Erratum: Phys. Rev. D **85**, 079901 (2012). [CrossRef]
21. H. N. Li, C. D. Lu, and F. S. Yu, *Branching ratios and direct CP asymmetries in $D \to PP$ decays*, Phys. Rev. D **86**, 036012 (2012). [CrossRef]
22. Y. Grossman, A. L. Kagan, and Y. Nir, *New physics and CP violation in singly Cabibbo-suppressed D decays*, Phys. Rev. D **75**, 036008 (2007). [CrossRef]
23. Y. Grossman, A. L. Kagan, and J. Zupan, *Testing for new physics in singly Cabibbo-suppressed D decays*, Phys. Rev. D **85**, 114036 (2012). [CrossRef]
24. I. I. Bigi, *Probing CP asymmetries in charm baryons decays*, arXiv:1206.4554 (2012). [CrossRef]
25. Y. Ünal and U.-G. Meißner, *Strong CP violation in spin-1/2 singly charmed baryons*, JHEP **01**, 115 (2021). [CrossRef]
26. Y. Grossman and S. Schacht, *U-spin sum rules for CP asymmetries of three-body charmed baryon decays*, Phys. Rev. D **99**, 033005 (2019). [CrossRef]
27. D. Wang, *Sum rules for CP asymmetries of charmed baryon decays in the $SU(3)_F$ limit*, Eur. Phys. J. C **79**, 429 (2019). [CrossRef]
28. M. Abumusabh *et al.* (Belle and Belle II Collaborations), *Search for CP violation in $\Xi_c^+ \to \Sigma^+ h^+ h^-$ and $\Lambda_c^+ \to p h^+ h^-$ decays at Belle II*, arXiv:2509.25765 [hep-ex]. [CrossRef]
29. K. Akai *et al.*, *Commissioning of KEKB*, Nucl. Instrum. Meth. A **499**, 191–227 (2003). [CrossRef]
30. A. Abashian *et al.* (Belle Collaboration), *The Belle Detector*, Nucl. Instrum. Meth. A **479**, 117–232 (2002). [CrossRef]
31. J. Brodzicka *et al.* (Belle Collaboration), *Physics Achievements from the Belle Experiment*, Prog. Theor. Exp. Phys. **2012**, 04D001 (2012). [CrossRef]
32. K. Abe *et al.* (Belle Collaboration), *Observation of large CP violation in the neutral B meson system*, Phys. Rev. Lett. **87**, 091802 (2001). [CrossRef]
33. T. Abe *et al.* (Belle II Collaboration), *Belle II Technical Design Report*, arXiv:1011.0352 [physics.ins-det] (2010). [arXiv]
34. W. Altmannshofer *et al.* (Belle II Collaboration), *The Belle II Physics Book*, Prog. Theor. Exp. Phys. **2019**, 123C01 (2019). [CrossRef]
35. The Belle II Collaboration, *Measurement of the integrated luminosity of data samples collected during 2019–2022 by the Belle II experiment*, arXiv:2407.00965 [hep-ex]. [CrossRef]
36. S. Navas *et al.* (Particle Data Group), *Review of Particle Physics*, Phys. Rev. D **110**, 030001 (2024). [CrossRef]
37. J. G. Körner and M. Krämer, *Exclusive nonleptonic charm baryon decays*, Z. Phys. C **55**, 659 (1992). [CrossRef]
38. M. A. Ivanov, J. G. Körner, V. E. Lyubovitskij, and A. G. Rusetsky, *Exclusive nonleptonic decays of bottom and charm baryons in a relativistic three-quark model: Evaluation of nonfactorizing diagrams*, Phys. Rev. D **57**, 5632 (1998). [CrossRef]
39. Q. P. Xu and A. N. Kamal, *Cabibbo-favored nonleptonic decays of charmed baryons*, Phys. Rev. D **46**, 270 (1992). [CrossRef]
40. H. Y. Cheng and B. Tseng, *Cabibbo-allowed nonleptonic weak decays of charmed baryons*, Phys. Rev. D **48**, 4188 (1993). [CrossRef]
41. P. Żenczykowski, *Nonleptonic charmed baryon decays: Symmetry properties of parity-violating amplitudes*, Phys. Rev. D **50**, 5787 (1994). [CrossRef]

 doi:10.20944/preprints202602.0472.v1

42. J. Q. Zou, F. R. Xu, G. B. Meng, and H. Y. Cheng, *Two-body hadronic weak decays of anti-triplet charmed baryons*, Phys. Rev. D **101**, 014011 (2020). [CrossRef]
43. K. K. Sharma and R. C. Verma, *A study of weak mesonic decays of Λ_c and Ξ_c baryons on the basis of HQET results*, Eur. Phys. J. C **7**, 217 (1999). [CrossRef]
44. C. Q. Geng, Y. K. Hsiao, C. W. Liu, and T. H. Tsai, *Anti-triplet charmed baryon decays with SU(3) flavor symmetry*, Phys. Rev. D **97**, 073006 (2018). [CrossRef]
45. C. Q. Geng, C. W. Liu, and T. H. Tsai, *Asymmetries of anti-triplet charmed baryon decays*, Phys. Lett. B **794**, 19 (2019). [CrossRef]
46. F. Huang, Z. P. Xing, and X. Z. He, *A global analysis of charmless two body hadronic decays for anti-triplet charmed baryons*, JHEP **03** (2022) 143. [CrossRef]
47. H. Zhong, F. Xu, Q. Wen, and Y. Gu, *Weak decays of anti-triplet charmed baryons from the perspective of flavor symmetry*, JHEP **02** (2023) 235. [CrossRef]
48. Z. P. Xing, X. Z. He, F. Huang, and C. Yang, *Global analysis of measured and unmeasured hadronic two-body weak decays of anti-triplet charmed baryons*, Phys. Rev. D **108** (2023) 053004. [CrossRef]
49. Z. P. Xing, Y. J. Shi, J. Sun, and Y. Xing, *SU(3) symmetry analysis in charmed baryon two body decays with penguin diagram contribution*, Eur. Phys. J. C **84**, 1014 (2024), [CrossRef]
50. H. J. Zhao, Y. L. Wang, Y. K. Hsiao, and Y. Yu, *A diagrammatic analysis of two-body charmed baryon decays with flavor symmetry*, JHEP **02** (2020) 165. [CrossRef]
51. Y. K. Hsiao, Y. L. Wang, and H. J. Zhao, *Equivalent $SU(3)_f$ approaches for two-body anti-triplet charmed baryon decays*, JHEP **09** (2022) 35. [CrossRef]
52. H. Zhong, F. Xu, and H. Y. Cheng, *Analysis of hadronic weak decays of charmed baryons in the topological diagrammatic approach*, Phys. Rev. D **109**, 114027 (2024). [CrossRef]
53. C. Q. Geng, X. G. He, X. N. Jin, C. W. Liu, and C. Yang, *Complete determination of $SU(3)_f$ amplitudes and strong phase in $\Lambda_c^+ \to \Xi^0 K^+$*, Phys. Rev. D **109** L073102 (2024). [CrossRef]
54. C. W. Liu, *Nonleptonic two-body weak decays of charmed baryons*, Phys. Rev. D **109** (2024) 033004. [CrossRef]
55. K. W. Edwards *et al.* (CLEO Collaboration), *Observation of new decay modes of the charmed-strange baryon Ξ_c^+*, Phys. Lett. B **373** (1996) 691. [CrossRef]
56. M. Ablikim *et al.* (BESIII Collaboration), *Measurement of the branching fraction for $\Lambda_c^+ \to pK^-\pi^+$*, Phys. Rev. Lett. **118**, 112001 (2017). [CrossRef]
57. M. S. Alam *et al.* (CLEO Collaboration), *Measurement of Cabibbo-suppressed decays of the Λ_c^+ baryon*, Phys. Rev. D **57**, 4467–4470 (1998). [CrossRef]
58. C. D. Lü, W. Wang, and F. S. Yu, *Test flavor SU(3) symmetry in exclusive Λ_c decays*, Phys. Rev. D **93**, 056008 (2016). [CrossRef]
59. M. Gronau, J. L. Rosner, and C. G. Wohl, *Isospin analysis of charmed baryon decays*, Phys. Rev. D **98**, 073003 (2018). [CrossRef]
60. L. K. Li *et al.* (Belle Collaboration), *Measurement of branching fractions of $\Lambda_c^+ \to pK_S^0K_S^0$ and $\Lambda_c^+ \to pK_S^0\eta$ at Belle*, Phys. Rev. D **107**, 032004 (2023). [CrossRef]
61. J. Y. Lee *et al.* (Belle Collaboration), *Measurement of branching fractions of $\Lambda_c^+ \to \eta\Lambda\pi^+$, $\eta\Sigma^0\pi^+$, $\Lambda(1670)\pi^+$, and $\eta\Sigma(1385)^+$*, Phys. Rev. D **103**, 052005 (2021). [CrossRef]
62. S. B. Yang *et al.* (Belle Collaboration), *Observation of a threshold cusp at the $\Lambda\eta$ threshold in the pK^- mass spectrum with $\Lambda_c^+ \to pK^-\pi^+$ decays* Phys. Rev. D **108**, L031104 (2023). [CrossRef]
63. K. Abe *et al.* (Belle Collaboration), *Observation of $B^\pm \to p\bar{p}K^\pm$*, Phys. Rev. Lett. **88**, 181803 (2002). [CrossRef]
64. M. Z. Wang *et al.* (Belle Collaboration), *Observation of $B^+ \to p\bar{p}\pi^+$, $B^0 \to p\bar{p}K^0$, and $B^+ \to p\bar{p}K^{*+}$*, Phys. Rev. Lett. **92**, 131801 (2004). [CrossRef]
65. B. Aubert *et al.* (BaBar Collaboration), *Measurement of the $B^+ \to p\bar{p}K^+$ branching fraction and study of the decay dynamics*, Phys. Rev. D **72**, 051101 (2005). [CrossRef]
66. R. Aaij *et al.* (LHCb Collaboration), *Observation of charmless baryonic decays $B^0_{(s)} \to p\bar{p}h^+h'^-$*, Phys. Rev. D **96**, 051103 (2017). [CrossRef]
67. R. Chistov, *Baryonic B Decays*, J. Phys. Conf. Ser. **675**, 022007 (2016). [CrossRef]
68. X. Huang, Y.-K. Hsiao, J. Wang, and L. Sun, *Baryonic B meson decays*, Adv. High Energy Phys. **2022**, 4343824 (2022). [CrossRef]
69. A. J. Bevan *et al.* (Belle Collaboration), *The Physics of the B Factories*, Eur. Phys. J. C **74**, 3026 (2014). [CrossRef]
70. V. Gabyshev *et al.* (Belle Collaboration), *Observation of the Decay $\bar{B}^0 \to \Lambda_c^+ \bar{p}$*, Phys. Rev. Lett. **90**, 121802 (2003). [CrossRef]

 doi:10.20944/preprints202602.0472.v1

71. Y. Ushiroda *et al.* (Belle Collaboration), *Time-dependent CP asymmetries in $B^0 \to K^0_s \pi^0 \gamma$ transitions*, Phys. Rev. D **74**, 111104 (2006). [CrossRef]
72. B. Aubert *et al.* (BaBar Collaboration), *Study of $\bar{B} \to \Xi_c \bar{\Lambda}_c^-$ and $\bar{B} \to \Lambda_c^+ \bar{\Lambda}_c^- K$ decays at BABAR*, Phys. Rev. D **77**, 031101 (2008). [CrossRef]
73. H.-Y. Cheng, *Exclusive baryonic B decays circa 2005*, Int. J. Mod. Phys. A **21**, 4209–4232 (2006). [CrossRef]
74. H. Y. Cheng, C. K. Chua, and S. Y. Tsai, *Doubly charmful baryonic B decays*, Phys. Rev. D **73**, 074015 (2006). [CrossRef]
75. H. Y. Cheng, C. K. Chua, and Y. K. Hsiao, *Study of $\bar{B} \to \Lambda_c \bar{\Lambda}_c$ and $\bar{B} \to \Lambda_c \bar{\Lambda}_c K$*, Phys. Rev. D **79**, 114004 (2009). [CrossRef]
76. C. H. Chen, *Production of doubly-charmed baryons in B decays*, Phys. Lett. B **638**, 214 (2006). [CrossRef]
77. Z. Rui, Z. T. Zou, and Y. Li, *Higher twist corrections to doubly-charmed baryonic B decays*, J. High Energy Phys. **12**, 159 (2024). [CrossRef]
78. V. L. Chernyak and I. R. Zhitnitsky, *B-meson exclusive decays into baryons*, Nucl. Phys. B **345**, 137–172 (1990). [CrossRef]
79. P. Ball and H. G. Dosch, *Branching ratios of exclusive decays of bottom mesons into baryon-antibaryon pairs*, Z. Phys. C **51**, 445 (1991). [CrossRef]
80. Y. K. Hsiao, *Study of two-body doubly charmful baryonic B decays with SU(3) flavor symmetry*, J. High Energy Phys. **11**, 117 (2023). [CrossRef]
81. H. Y. Cheng, *Status of baryonic B decays*, Nucl. Phys. B **Suppl. 163**, 68 (2007). [CrossRef]
82. R. C. Verma, *SU(3) flavor analysis of nonfactorizable contributions to $D \to PP$ decays*, Phys. Lett. B **365**, 377–382 (1996). [CrossRef]
83. A. C. Katoch, K. K. Sharma, and R. C. Verma, *Isospin analysis of non-factorizable contributions to hadronic decays of charm mesons*, J. Phys. G: Nucl. Part. Phys. **23**, 807 (1997). [CrossRef]
84. A. N. Kamal, A. B. Santra, T. Uppal, and R. C. Verma, *Nonfactorization in hadronic two-body Cabibbo-favored decays of D^0 and D^+*, Phys. Rev. D **53**, 2506 (1996). [CrossRef]
85. M. Kaur and R. C. Verma, *SU(3) analysis of nonfactorizable contributions to bottom mesons decays*, J. Subatomic Part. Cosmol. **3**, 100033 (2025). [CrossRef]
86. R. Aaij *et al.* (LHCb Collaboration), *A measurement of the CP asymmetry difference in $\Lambda_c^+ \to pK^-K^+$ and $\Lambda_c^+ \to p\pi^-\pi^+$ decays*, JHEP **03**, 182 (2018). [CrossRef]
87. F. A. Berends, K. J. F. Gaemers, and R. Gastmans, *α^3 contribution to the angular asymmetry in $e^+e^- \to \mu^+\mu^-$*, Nucl. Phys. B **63**, 381 (1973). [CrossRef]
88. R. W. Brown, K. O. Mikaelian, V. K. Cung, and E. A. Paschos, *Electromagnetic background in the search for neutral weak currents via $e^+e^- \to \mu^+\mu^-$*, Phys. Lett. B **43**, 403 (1973). [CrossRef]
89. R. J. Cashmore, C. M. Hawkes, B. W. Lynn, and R. G. Stuart, *The forward–backward asymmetry in $e^+e^- \to \mu^+\mu^-$: comparisons between theoretical calculations at the one-loop level in the Standard Model and with the experimental measurements*, Z. Phys. C **30**, 125 (1986). [CrossRef]
90. Belle II Collaboration, *Belle II Collaboration Homepage*, [CrossRef].